A 12,000-year dinoflagellate cyst record on the Vancouver Island Margin, Canada: tracing past climatic, primary productivity and oceanographic conditions

Zhen Li[a,b,*], Vera Pospelova[c], Kenneth Neil Mertens[d], Alice S. Chang[b], Yongsheng Wu[f]

[a] Geological Survey of Canada-Pacific, Natural Resources Canada, 9860 W. Saanich Road, Sidney, British Columbia, V8L 4B2, Canada

[b] Department of Earth, Ocean and Atmospheric Sciences, University of British Columbia, 2020–2207 Main Mall, Vancouver, British Columbia, V6T 1Z4, Canada

[c] Department of Earth and Environmental Sciences, University of Minnesota, 116 Church St SE, Minneapolis, MN, 55455, USA

[d] Ifremer, COAST, F-29900, Concarneau, France

[e] Fisheries and Oceans Canada, Bedford Institute of Oceanography, 1 Challenger Drive, Dartmouth, Nova Scotia, B2Y 4A2, Canada

*Corresponding author:

Zhen Li (Zhen.Li2@nrcan-rncan.gc.ca or imlizhen@hotmail.com)

Abstract

This study investigated dinoflagellate cyst records spanning the latest Pleistocene to the late Holocene on the Vancouver Island margin, identifying 14 autotrophic and 26 heterotrophic taxa. Four dinoflagellate cyst zones were defined and related to paleoclimatic and paleoceanographic conditions. Zone I (~14–~11.6 cal kyr BP) showed the lowest primary productivity (PP), indicated by the lowest total cyst concentrations, with *Brigantedinium* spp. dominant in assemblages. This was likely due to cooler conditions associated with glacial meltwater input and/or weak coastal upwelling. Zone II (~11.6–~10.6 cal kyr BP) showed a slight increase in total cyst concentrations, a rapid increase in *Operculodinium centrocarpum* sensu Wall and Dale 1966 and the highest *Nematosphaeropsis labyrinthus* abundances. This zone was linked to reduced meltwater input and increased coastal upwelling, promoting primary productivity. Zone III (~11.6–~8.2 cal kyr BP) showed a rapid increase in PP, with total cyst concentrations peaking and autotrophic taxa reaching their highest abundances. This was associated with strengthened California Undercurrent and increased upwelling, coinciding with the highest insolation intensity. The high *Impagidinium* abundances indicated more open ocean conditions. A sharp increase in *Operculodinium centrocarpum*-truncate processes during ~9–8.2 cal kyr BP may be related to the 8.2 ka event and decelerated sea-level rise. Zone IV (~8.2–~2.3 cal kyr BP) indicated gentle fluctuations in PP, with an overall total cyst concentrations decline, reaching the lowest around 8.0 cal kyr BP, followed by a slight increase at ~6.5 cal kyr BP, and subsequent stabilization.

Keywords: Dinoflagellate cysts, Holocene, Post glaciation, Deglaciation, Climatic changes Paleoceanography, Paleoenvironment, Offshore of Vancouver Island, Northeastern Pacific Ocean

1. Introduction

Extensive research has been conducted on late Quaternary climate, oceanography, and primary productivity (PP) along the western margin of North America (e.g., Pisias et al., 2001; Barron et al., 2003, 2022; Friddell et al., 2003; Pospelova et al., 2006, 2015; Barron and Bukry, 2007; Fisler and Hendy, 2008; Price et al., 2013; McGann, 2015; Addison et al., 2018; Over and Pospelova, 2022; Palmer et al., 2023). These studies have provided insights into the history of major climatic and oceanographic changes, marine productivity, and ecosystem events, along with their primary control factors during the Quaternary period. However, this collective research has primarily focused on the California Current System off the west coast of the United States. In contrast, Holocene studies on the influence of the California Current System and marine ecosystems off western Canada remain limited.

The modern southwest coast of Vancouver Island is highly productive and rich in fisheries resources (e.g., Antoine et al., 1996; Ware and Thomson, 2005). Earlier studies of sediment cores from the Vancouver Island margin have revealed that oceanographic conditions and marine production have varied over time and on different spatial and temporal scales. Kienast and McKay (2001) reconstructed a history of sea-surface temperature (SST) over the last 16,000 years based on alkenone unsaturation ratios (Uk'37) and noted that SST ranged from ~6°C to ~12°C between 16 and 11 cal kyr BP. Using geochemical proxies, McKay et al. (2004) and Chang et al. (2008) reported higher marine export production during the Holocene and lower production during glacial periods. McKay et al. (2005) suggested that the oxygen minimum zone (OMZ) off Vancouver Island was more intense, relative to modern conditions, during the intervals of 13.5–12.6 cal kyr BP and 11–10 cal kyr BP due to increased organic matter export. During the Holocene, marine organic carbon, the main contributor to total organic carbon (TOC), increased, whereas terrestrial

63 organic carbon decreased, compared to glacial periods, when more terrestrial organic carbon was
64 deposited onto the margin (Chang et al., 2008). In addition, these authors suggested that ^{15}N-
65 enriched nitrate generated in the Eastern Tropical North Pacific (ETNP) could be transported
66 northward by the California Undercurrent to the Vancouver Island margin. Collectively, these
67 studies contributed to a regional perspective by illustrating broad variations in marine productivity
68 and oceanographic conditions that corresponded to climatic fluctuations on glacial-interglacial
69 time scales. However, short-term climatic shifts, variations in current strength and routes, and
70 consequently fluctuations in marine PP during specific intervals of the Holocene remain undefined.
71 Moreover, the organic carbon content in marine sediments used in these studies reflects marine
72 export production (e.g., Calvert and Pedersen, 1992), which is not wholly indicative of PP and
73 surface-ocean conditions.

74 Dinoflagellates represent a major planktonic group that contributes to modern marine PP.
75 Many dinoflagellate species produce organic-walled cysts, which are resistant to physical,
76 chemical, and biological degradation, and therefore become well preserved in the sediments (e.g.,
77 Dale, 1996). The distributions of modern dinoflagellate cysts are controlled by SST, sea-surface
78 salinity (SSS), PP, nutrients, sea-ice cover, and other oceanographic conditions (e.g., Dale, 1996;
79 Rochon et al., 1998; de Vernal et al., 2001, 2020; Marret Zonneveld, 2003; Pospelova et al., 2005,
80 2008; Pospelova Kim, 2010; Price Pospelova, 2011; Bringué et al., 2013; Zonneveld et al., 2013;
81 Gurdebeke et al., 2018; Li et al., 2018, 2020, 2023). Therefore, organic-walled dinoflagellate cysts
82 preserved in sediments have been successfully used for reconstructing past oceanographic
83 conditions across the Pacific Ocean (e.g., Lewis et al., 1990; Marret et al., 2001; Mudie et al.,
84 2002; Pospelova et al., 2006, 2015; Verleye Louwye, 2010; Price et al., 2013; Limoges et al., 2014;
85 Li et al., 2017, 2021). Dinoflagellate cyst-based reconstructions from sediment cores from the west

coast of Canada have been primarily limited to the coastal inlets of Vancouver Island. For example, using dinoflagellate cysts in Effingham Inlet, Patterson et al. (2011) quantitatively reconstructed winter SST over the last 5,500 years, and Bringué et al. (2016) provided a high-resolution reconstruction of the sedimentary environment and changes in SST, SSS and PP over the last 1,000 years.

The sediment core MD02-2496, collected from the Vancouver Island margin, presents the first opportunity to illustrate a high-resolution dinoflagellate cyst record and to reconstruct a cyst-based marine paleoenvironmental history that extends back to the late Pleistocene. This core is well-dated and well-characterized for grain size (Cosma and Hendy, 2008), geochemical proxies for productivity (Chang et al., 2008), and redox geochemistry (Chang et al., 2014). In this paper, we focus on the core's upper section, which spans the last 14,000 years, when the Cordilleran Ice Sheet (CIS) had already retreated from the shelf (Clague and James, 2002). Furthermore, we compare the record from the Vancouver Island margin with other regions along the western margin of North America to gain insights into the mechanisms that governed how the planktonic ecosystem and PP responded to regional climatic, oceanographic, and sea-level changes.

2. Regional Setting

2.1. Geography and Geology

The continental shelf off Vancouver Island extends from the coastline to ~200 m water depth (Fig. 1). The width of the shelf varies from ~6 km, at Brook's Peninsula, to ~95 km, at the mouth of the Juan de Fuca Strait (Fig. 1; Kung et al., 2023). During the last glaciation, the CIS advanced from the Coast Mountains on the British Columbian mainland, overtopped Vancouver Island, and reached a maximum extent at ~15 ^{14}C ka BP (16–17 cal kyr BP) at the end of the Last Glacial Maximum (LGM), when ice covered much of the continental shelf off Vancouver Island

(e.g., Clague and James, 2002). After the LGM, the CIS started to decay (e.g., Taylor et al., 2014), and the shelf off Vancouver Island became completely ice-free by ~13.5 ^{14}C ka BP (~15 cal kyr BP) (Dethier et al., 1995; Hewitt and Mosher, 2001; Hendy Cosma, 2008). By ~11–10.5 ^{14}C ka BP (~12–11.2 cal kyr BP), the ice sheet had receded to the Coast Mountains.

The growth and decay of the CIS significantly influenced the sedimentary environment on the shelf and slope off Vancouver Island. Ice sheet expansion led to increased glacial erosion on land, whereby the ice carried an abundance of poorly sorted terrestrial materials to the continental shelf. With rapid ice-sheet retreat at the beginning of the deglaciation, coarse sediments and ice-rifted debris (IRD) were released from the melting ice and resulted in higher mass accumulation rates over the shelf and slope (Cosma et al., 2008). As the ice retreated further to the mainland, the deposition of IRD and terrestrial sediments onto the shelf decreased until eventually no IRD was deposited (Cosma and Hendy, 2008).

2.2. Climate and Oceanography

The modern temperate climate off the west coast of Canada is controlled by the cyclonic Aleutian Low (AL) and the anti-cyclonic North Pacific High (NPH) pressure systems (e.g., Thomson, 1981). In winter, the AL pushes the NPH southward and generates southwesterly winds along the Vancouver Island west coast (Fig. 1; e.g., Thomson, 1981; Patterson et al., 2011). Through Ekman transport, the southwesternly wind pushes surface waters towards the shore. In summer, the NPH becomes the dominant pressure system, bringing northwesterly winds, generating a southward Shelf Break Current, and resulting in offshore transport of surface waters and persistent upwelling along the entire coast of Vancouver Island (Crawford and Thomson, 1991; Hickey and Banas, 2008).

Off the west coast of Canada today, the bifurcation of the Subarctic and North Pacific currents gives rise to the northward Alaska Current and the southward California Current (Fig. 1). In winter, the California Current is pushed offshore by the Davidson Current, a seasonal surface current that moves northwards from 32°N to the coast of Vancouver Island (Fig. 1). The Davidson Current occurs in winter and flows northwesterly along the coast, which is possibly formed (Thomson, 1981) or partially formed (Krassovski, 1993) by the California Undercurrent penetrating the ocean surface. The California Undercurrent is a strong, northward subsurface flow that originates off southern California and includes subtropical subsurface water from the ETNP. The Undercurrent flows all year round, following the continental slope at depths between 250–300 m, and extends as far north as Vancouver Island and even to southeast Alaska (e.g., Thomson and Krassovski, 2010). The Undercurrent reaches maximum speeds in the fall and winter (Thompson, 1981), with the strongest flow at depths of 100–300 m off Vancouver Island (Reed and Halpern, 1976).

Seasonal winds along the west coast of Vancouver Island also result in predominantly downwelling conditions during winter months and upwelling conditions during spring through to fall (e.g., Crawford and Thomson, 1991; Ware and Thomson, 2005). The upwelling transports cold and nutrient-rich waters from the bottom as well as California Undercurrent to the surface (e.g., Mackas et al. 1987). Along the shelf break, the lowest concentrations of bottom water oxygen are observed during summer due to the upwelling of nutrients and resultant high PP in surface waters and export productivity to the seafloor (e.g., Crawford and Thomson, 1991).

3. Materials and Methods

The 38.35-m-long, 10-cm diameter sediment core MD02-2496 (48° 58.47′N, 127° 02.14′W, 1243 m water depth) was collected in 2002 on the R/V Marion Dufresne, using a giant

Calypso piston corer (Fig. 1). The chronology of the core was established with 46 AMS ^{14}C measurements. All ^{14}C ages (yr BP) were converted into calibrated years (cal yr BP) by Cosma et al. (2008) using CALIB04 (Stuiver et al., 2004). Reservoir-corrected ^{14}C dates for planktonic foraminiferal samples younger than 22 ^{14}C kyr BP were calibrated using MARINE04 (Hughen et al., 2004). Bulk organic carbon samples were corrected using both MARINE04 and INTCAL04 (Reimer et al., 2004) and a reservoir age based on the percentage of terrestrial organic carbon in each sample (Cosma et al., 2008). The bottom of the core was dated to ~50,000 cal yr BP. The top section of the core was lost, which is common for piston coring, and the youngest sediment was dated at ~2.25 cal kyr BP. For the present study, we focus on the section of the core above 560 cm (calibrated depth), which spans back to 13.86 cal kyr BP (Fig. 2). This section is mainly composed of olive grey clayey silt, with the sediment fraction constituting 21–70% silt (10–63 μm) and 10–26% clay (<2–4 μm). Sand (>63 μm) is sporadically present (<1%), except for a notable peak of ~4% of the sediment fraction at ~12.5 cal kyr BP (Cosma and Hendy, 2008).

A total of 51 samples for dinoflagellate cyst analysis were taken at 10 cm intervals from the working half of the core, with each sample being 1 cm in thickness. All samples were treated using a standard palynological processing technique described in Pospelova et al. (2005, 2010) to extract dinoflagellate cysts from sediments. One tablet of dyed *Lycopodium clavatum* grains (27,560 grains per tablet) was added to each sample to estimate cyst concentrations. Carbonates and silicates were then removed from the samples with 10% HCl and 48% HF at room temperature, respectively. Sieving through a 120-μm and a 15-μm Nitex nylon mesh eliminated coarser and finer particles, respectively. Gentle sonication for up to 1 min was applied before collecting the residue on a 15-μm nylon mesh. The residues were strew-mounted on slides using glycerine jelly for subsequent microscopy observations.

Dinoflagellate cysts were identified and counted using Nikon Eclipse optical microscopes (models 80i and E200) at 500x, 600x and 1000x magnifications, and high-quality images were captured using a Nikon Digital Sight DS-L2 imaging controller. Over 300 dinoflagellate cysts were counted in each sample. Dinoflagellate cyst identification and determination of their biological affinities were based on the descriptions of Esper and Zonneveld (2002), Gurdebeke et al. (2020a, 2020b, 2021), Li et al. (2023); Matsuoka (1988), Matsuoka et al. (2009), Mertens et al. (2020), Rochon et al. (1999), Van Nieuwenhove et al. (2020), and Zonneveld and Pospelova (2015). Cysts were identified at the species level whenever possible. Some cyst taxa, where morphological similarities made species-level identification challenging, were identified to their genus level and expressed as their genus name with "spp.". Specifically, smooth, round brown cysts with an archeopyle were grouped as *Brigantedinium* spp, while undetermined brown cysts with obscured horns were grouped as cysts of *Protoperidinium* spp. Undetermined round brown spiny cysts without an obscured split or archeopyle were grouped as round brown spiny cysts (RBSCs). Cysts produced by autotrophic and heterotrophic dinoflagellates were labeled, respectively.

The relative abundances of each dinoflagellate cyst taxon were calculated as percentages of the total cysts counted in each sample. Dinoflagellate cyst concentrations were calculated as the number of cysts per gram of each dried sample (cysts g^{-1}). Diagrams of downcore plots of dinoflagellate cyst abundances were created with Tilia 1.5.12 software. Dinoflagellate zones and subzones were determined through stratigraphically constrained cluster analysis (CONISS) conducted on the relative abundances of all taxa, from which square root transformations and Edwards and Cavalli-Sforza's chord distances were chosen to be dissimilarity coefficients (Grimm, 1991, 1992). Principal components analysis (PCA), performed with CANOCO 5 software (Ter Braak and Smilauer, 2012), was applied to logarithmically transformed relative abundances of

dinoflagellate cysts to identify major trends in the assemblages. We further conducted redundancy analysis (RDA) on data of dinoflagellate cysts, using geochemical data from Chang et al. (2008, 2014) as environmental parameters.

Considering the cysts preserved in the sediment core come from a larger area of surface water rather than a parcel of water directly above the core site, we utilized a web-based tool (https://planktondrift.science.uu.nl; Nooteboom et al., 2019) to trace the potential geographic sources of the cysts, assuming similarity to modern hydrographic conditions. This tool uses a backward particle tracking method that integrates velocity, time, and source location. The velocity data included ocean currents derived from the Ocean General Circulation Model for the Earth Simulator (OFES) (Ohfuchi et al., 2004; Sasaki et al., 2008), which is a global, three-dimensional circulation model that has a horizontal resolution of 1/10° and 54 vertical levels. From the aggregation properties of dinoflagellate cysts during their transport from surface waters to the sediments, we assumed a sinking velocity of 6 m day^{-1} (Anderson et al., 1985).

4. Results

4.1. Dinoflagellate cyst concentrations and assemblages

A total of 40 dinoflagellate cyst taxa were identified in 51 samples from core MD02-2496 (Table 1, Plates I-IV). Total cyst concentrations varied from 734 to 14,482 cysts g^{-1} per sample, with an average of 6,070 cysts g^{-1} (Fig. 2). Four dinoflagellate cyst zones (I to IV) and five subzones (IIIa to IVc) were determined based on CONISS results (Fig. 2a).

Zone I (~14 to ~11.6 cal kyr BP) was characterized by low total cyst concentrations (734–2593 cysts g^{-1}), with high relative abundances of heterotrophic taxa (83.3–94.8%) and high ratios of heterotrophic to autotrophic taxa (H/A) from 5 to 18.3. In the cyst assemblages, *Brigantedinium* taxa were predominant (49.7–72.1%, 386–1665 cysts g^{-1}), consisting largely of unidentified

Brigantedinium spp. (~46%, ~819 cysts g^{-1}) and *Brigantedinium simplex* (~13.65%, 254 cysts g^{-1}), and low abundances of *Brigantedinium cariacoense*. Cysts of *Protoperidinium* spp. were also a common contributor to the heterotrophic taxa (8.1–12.2%, 79–288 cysts g^{-1}), followed by the abundances of *Islandinium pacificum* (2.3–8.5%, 26–183 cysts g^{-1}). Other heterotrophic taxa had lower abundances, such as *Quinquecuspis concreta* (~2.8%, ~16 cysts g^{-1}), cysts of *Polykrikos schwartzii* (~1.9%, ~28 cysts g^{-1}), *Selenopemphix undulata* (~1.5%, ~25 cysts g^{-1}), *Dubridinium cavatum* (~1.3%, ~23 cysts g^{-1}), *Selenopemphix quanta* (~1.1%, ~19 cysts g^{-1}), and *Votadinium spinosum* (0.5%, ~9 cysts g^{-1}).

Autotrophic taxa had the lowest abundances in Zone I, with percentages of ~11.3% and concentrations of ~195 cysts g^{-1}, which averaged to about one-tenth of the abundance of the heterotrophic taxa (Fig. 2). Autotrophic taxa commonly consisted of *Operculodinium centrocarpum* sensu Wall and Dale 1966 (~7.4%, 131 cysts g^{-1}). Other species appeared in low abundances (<3%, <20 cysts g^{-1}), such as *Spiniferites elongatus*, *Spiniferites ramosus*, *Spiniferites* spp., cysts of *Pentapharsodinium dalei*, *Hiddenocysta matsuokae*, *Nematosphaeropsis labyrinthus*, and *Operculodinium centrocarpum*-truncate processes. Zone I had high positive scores for PCA1 and low positive scores for PCA2 (Fig. 2a).

Zone II (~11.6 – ~10.6 cal kyr BP) was distinguished by a notable increase in the relative abundances of autotrophic taxa and a decrease in heterotrophic taxa, along with the highest abundances of *Nematosphaeropsis labyrinthus* (~2.4%, 64 cysts g^{-1}) in the entire studied section (Fig. 2). As a result, H/A ratios decreased to 1–9 from Zone I. The average abundances of *Operculodinium centrocarpum* sensu Wall and Dale 1966 increased to ~29.3% and 1586 cysts g^{-1}, whereas the abundances of *Brigantedinium* spp. decreased to ~26.4% and 1330 cysts g^{-1}. *Islandinium pacificum* slightly decreased to 0.9–5.6% and 39–226 cysts g^{-1}. *Votadinium* species

became rare. Both PCA1 and PCA2 had positive scores in this zone, although PCA1 scores were slightly lower than in Zone I and PCA2 scores were much higher than in Zone I.

Zone III (~10.6 – ~8.2 cal kyr BP) was characterized by the highest abundances of autotrophic taxa and the lowest heterotrophic taxa, as reflected in the lowest H/A ratio of 0.4 (Fig. 2). Total cyst concentrations reached the highest value of 14,482 cysts g^{-1} at ~10.35 cal kyr BP and then declined. The abundances of *Spiniferites* spp. increased to 1.3–4.4% and 152–599 cysts g^{-1}. *Hiddenocysta matsuokae* reached their highest abundances of 2.2% and 237 cysts g^{-1} at ~10.1 cal kyr BP. *Impagidinium* taxa started to appeare at ~10.6 cal kyr BP, mainly consisting of *Impagidinium aculeatum*, although total *Impagidinium* abundances were <5% and <200 cysts g^{-1}. Subzone IIIa (~10.6 – ~9.0 cal kyr BP) was distinguished by the highest abundances of *Operculodinium centrocarpum* sensu Wall and Dale 1966 and the lowest total *Brigantedinium*, whereas Subzone IIIb (~9.0 – ~8.2 cal kyr BP) had the highest abundances of *Operculodinium centrocarpum*-truncate processes, with peak values of 30.7% and 3101 cysts g^{-1} at ~8.8 cal kyr BP. In this subzone, total *Brigantedinium* abundance increased again. In the entire studied section, Zone III had the highest negative scores for PCA1, whereas Subzone IIIb had the highest positive scores for PCA2.

Zone IV (~8.2 – ~2.3 cal kyr BP) was characterized by similar relative abundances of autotrophic taxa and heterotrophic taxa, with an average H/A ratio of 1.2 (Fig. 2). The two most dominant taxa in this zone showed opposite trends in their relative abundances: *Operculodinium centrocarpum* sensu Wall and Dale 1966 slightly increased toward 6.5 cal kyr BP and then declined after, whereas total *Brigantedinium* decreased before 6.5 cal kyr BP and then slightly increased thereafter. The abundances of *Brigantedinium* spp. and *Brigantedinium simplex* were relatively stable. *Operculodinium centrocarpum*-truncate processes decreased sharply in concentration from

Subzone IIIb, then appeared sparsely throughout Zone IV. The abundances of *Dubridinium cavatum*, *Echinidinium* spp., cysts of Diplopsalid, and *Islandinium pacificum* increased relative to Subzone IIIb.

Subzone IVa (~8.2 – ~6.5 cal kyr BP) was distinguished from other subzones by increases in the abundances of autotrophic taxa. Total cyst concentrations were lowest at ~8 cal kyr BP. The abundances of total *Spiniferites* reached the highest values of 17.6% and 949 cysts g^{-1} at 7.1–6.7 cal kyr BP, mainly contributed by *Spiniferites ramosus* (~10.5%, ~543 cysts g^{-1}) and *Spiniferites* spp. (~6.7%, ~387 cysts g^{-1}). Heterotrophic taxa slightly decreased in relative abundance, but gradually increased in their concentrations. *Echinidinium* spp. and *Quinquecuspis concreta* both reached their highest relative abundances throughout the studied section, at ~8 cal kyr BP, and subsequently decreased. In this subzone, cysts of *Pentapharsodinium dalei* also reached their highest abundances (~2.7%, ~150 cysts g^{-1}) throughout the studied section.

Subzone IVb (~6.5 – ~4.0 cal kyr BP) had stable total cyst concentrations, but slightly increasing H/A ratios over time due to an increase in heterotrophic taxa and a decline in autotrophic taxa. The highest abundances of *Islandinium pacificum*, *Selenopemphix undulata*, and *Votadinium spinosum* distinguished IVb from Subzones IVa and IVc (~4 – 2.3 cal kyr BP).

Subzone IVc had a decline in total cyst concentrations and the highest abundances of *Echinidinium aculeatum* throughout the studied section. Undetermined RBSCs notably increased to the highest levels throughout the record after 2.7 cal kyr BP. H/A ratios reached higher values, with respect to other zones, since 10.6 cal kyr BP.

Scores for PCA1 were more negative in Subzone IVa than in IVb, but scores for PCA2 were less negative in Subzone IVa than in Subzones IVb and IVc. Scores for PCA1 and PCA2 were both negative in subzone IVc. Nevertheless, Subzones IVb and IVc were not well

distinguished by the PCA axes due to the high similarity in cyst assemblages, except for the notable increase in undetermined RBSCs in Subzone IVc.

4.2. PCA and RDA results

The first principal component of the PCA (PCA1) explained 27.67% of the variance in the dinoflagellate cyst data (Fig. 3a). Along the axis of PCA1, *Brigantedinium* spp., *Brigantedinium simplex*, and *Lejeunecysta sabrina* had more affinity with samples of Zone I. *Brigantedinium* spp., *Brigantedinium simplex*, cysts of *Polykrikos schwartzii, Quinquecuspis concreta*, and *Lejeunecysta sabrina* had high positive scores, which distinguished the samples within Zones I and II from other samples. In contrast, *Operculodinium centrocarpum* sensu Wall and Dale 1966, *Spiniferites* spp., and *Spiniferites ramosus* showed high negative scores.

The second principal component (PCA2) explained 19.49% of the variance in the cyst data. *Operculodinium centrocarpum*-truncate processes, *Impagidinium aculeatum*, and *Hiddenocysta matsuokae* were positively loaded on the PCA2 axis. The samples from Zone III were positively correlated with these species with high PCA2 scores. Most of the heterotrophic taxa, such as cysts of *Protoperidinium* spp., *Islandinium pacificum*, *Echinidinium aculeatum*, *Echinidinium* spp., undetermined RBSCs, cysts of Diplopsalid, *Selenopemphix quanta*, *Selenopemphix undulata*, *Dubridinium cavatum*, and *Votadinium calvum* were negatively loaded on the PCA2 axis and correspond to most samples from subzones IVb and IVc.

The first axis of RDA explained 23.49% of the variance, and the second axis explained 15.15% (Fig. 3b). Monte Carlo permutation tests indicated that concentrations of total nitrogen (TN), total organic carbon (TOC), molybdenum (Mo) and barium (Ba), isotope ratios of $\delta^{15}N_{bulk}$ and $\delta^{13}C_{org}$, and the ratios of Mn/Al and Mo/Al were significant environmental parameters (p <0.05; Fig. 3b). Ratios of Mn/Al were positively correlated with the first RDA axis. The

heterotrophic cysts of *Brigantedinium* spp., *Brigantedinium simplex*, *Quinquecuspis concreta,* and cysts of *Polykrikos schwartzii also* had high positive scores on the first axis (Fig. 3b). In contrast, TN, TOC and $\delta^{13}C_{org}$ were the most statistically significant parameters and pointed in the negative direction of the first RDA axis. The autotrophic taxa, including *Operculodinium centrocarpum* sensu Wall and Dale 1966, *Spiniferites ramosus*, and *Spiniferites* spp., had high negative scores of the first axis. Values for $\delta^{15}N_{bulk}$ pointed in the positive direction of the second RDA axis, with accompanying high scores for *Operculodinium centrocarpum*-truncate processes, *Impagidinium aculeatum* and *Hiddenocysta matsuokae*. Most of the heterotrophic taxa had negative scores on the second axis, with high scores for *Echinidinium* spp., cysts of *Protoperidinium* spp., and *Islandinium pacificum*.

5. Discussion

5.1. Main origin sources of dinoflagellate cysts

Dinoflagellate cyst records from sediment cores have been used for qualitative and quantitative paleoceanographic reconstructions based on the assumptions that the cysts originated from the surface water directly above, where the corresponding motile stage is present, and the sources have not changed in study time intervals. However, cysts, which lack mobility, are subjected to three-dimensional transport, including lateral transport by currents throughout the water column, before being deposited on the seafloor (e.g., Dale, 1976; Nooteboom et al., 2019). In shallow lagoonal settings (average water depth <2.1 m), lateral transport is not a factor and dinoflagellate cyst assemblages in surface sediments reflect the heterogeneity of upper water column conditions in estuaries (Pospelova et al., 2004). However, Nooteboom et al. (2019) modeled dinoflagellate cyst transport in a global model of the present-day ocean and invalidated the assumption that cysts or sedimentary particles represent only the directly overlying surface

waters. Thus, in more open-ocean environments, lateral transport should be considered because it can result in the redistribution of cysts along their sinking trajectory, where cysts deposited at a coring site could originate from both the water directly above (autochthonous) and from distal or surrounding surface waters (allochthonous) (e.g., Zonneveld et al., 2022).

Core MD02-2496 was collected at a depth of 1243 m (Fig. 1), on the upper continental slope off Vancouver Island, which is influenced by coastal upwelling and a variety of local and regional surface and subsurface ocean currents (Section 2.2). Utilizing the online trace simulation tool (Nooteboom et al., 2019), we illustrate that the potential present-day surface water sources of the deposited cysts cover a broad coastal area around the coring site, ranging from 50°29.76'N, 129°10.6'W in the northwest to 47°40.4'N, 125°11.2'W in the southeast (Fig. 1a). The main cyst sources are concentrated in the upper waters over the slope, both proximal and northwest of the coring site. The sources from the shelf are mainly from the southeast, off Barkley Sound and the mouth of Juan de Fuca Strait, although the exact proportions contributed from these regions remain undetermined. Therefore, the cysts in this core are likely to reflect PP and local ocean currents within a broader area over the continental margin off Vancouver Island (regional) rather than conditions directly above the core location (local).

On the other hand, the potential source locations of cysts in the past could also differ from the present day. For example, the retreat of the CIS suggests that all potential source locations were free of ice after ~14 cal kyr BP (Clague and James, 2002). Even so, glacial meltwater input from large ice caps on the mountains on Vancouver Island and from the CIS on the mainland could have affected the paths and strength of coastal currents or upwelling, due to density differences, futher impacting the potential origin sources of cysts. Therefore, before the complete disappearance of the large ice caps and the CIS at ~ 11–10.5 ka BP (~12–11.2 cal kyr BP), more

cysts from upper waters over the shelf could be delivered to the core location due to the input of large volumes of meltwaters from the mountains on Vancouver Island through submarine channels, such as in the Barkley Sound area, and from the mainland through the Strait of Juan de Fuca. By 9.5 ka BP (~10 cal kyr BP), the size of the glaciers in the Coast Mountains were likely similar to present conditions (Clague, 1981), after which we can assume that cyst sources began resembling present-day transport modeling. Nevertheless, estimating changes in the strength of ocean currents and their effects on sinking cysts over the studied time interval is challenging. However, at the very least, the difference in cyst sources during times with and without glacial meltwater input should be considered when interpreting cyst records in the sediment core.

5.2. Sedimentary environment and low PP during the latest Pleistocene (Zone I)

Relatively low PP prior to 11.6 cal ka BP was inferred from the lowest dinoflagellate cyst concentration in Zone I (Fig. 4). The lower PP could have resulted from weak upwelling during the transition to rapid deglaciation (e.g., McKay et al., 2005) because of large volumes of meltwater input and the cooler climate in the latest Pleistocene (especially Younger Dryas event, e.g., Pospelova et al., 2015) than that in the Holocene. During this time interval, ice still covered most of Vancouver Island, although the shelf was ice-free (Clague and James, 2002). Meltwater from the mountains on Vancouver Island flowed into the ocean through channels or inlets along the west coast, while meltwater from the mainland entered through the Strait of Juan de Fuca. The meltwater from retreating glaciers could have created a stratified water column by forming a buoyant layer of freshwater over the denser saltwater, thus suppressing coastal upwelling along the shelf break. Deep nutrient-rich waters were less likely to reach the surface, thus limiting high PP.

In addition, isostatic rebound due to ice unloading caused a rapid fall in local sea level, as shown by the reconstructed sea-level curve of the Barkley Sound region (Fig. 4a; Dallimore et al., 2008). The sea-level fall resulted in increased erosion and enhanced inputs of terrestrial material, as indicated by the highest content of coarse sediment (>63 um, sand) in core MD02-2496 (Fig. 4n; Cosma and Hendy, 2008). The delivery of lithogenous and nutrient-poor materials to the shelf, along with large volumes of meltwater, likely created conditions that were not conducive to high PP. Additionally, the higher density of sandy sediment and the greater terrestrial input could have diluted the abundance of cysts on a per-mass basis in samples from this tive inteval.

Although the PP before 11.6 cal kyr BP was much lower compared to the early Holocene, a minor decrease in PP occurred, as reflected by a slight decrease in total cyst concentrations, from 2155 cysts g^{-1} at 13.87 cal kyr BP to 734 cysts g^{-1} at 12.66 cal kyr BP (Figs 2 and 4). This decrease might be associated with the transition from the Bølling-Allerød warm interval (14.7–12.9 cal kyr BP) to the Younger Dryas cool interval (12.9–11.7 cal kyr BP), two stages characterized in the latest Pleistocene (e.g., Barron et al., 2003; Behl and Kennett, 1996; Mathewes et al., 1993; McGann, 2011; Palmer et al., 2023; Pospelova et al., 2006, 2015). Chang et al. (2008) described the Younger Dryas in MD02-2496 as an interval containing depleted values of $\delta^{13}C_{org}$ and $\delta^{15}N_{bulk}$ (terrestrial organic matter), and decreased concentrations of carbonate, TOC, and opal (i.e., lower abundances of primary producers such as coccolithophores and diatoms, respectively), which are consistent with the low observed total cyst concentrations and low inferred PP in this study (Fig. 4). In nearby core JT96-09PC (Fig. 1a), Kienast and McKay (2001) inferred a drop in SST of ~3°C from the Allerød to the Younger Dryas based on C_{37} alkenone unsaturation. Similar declines in dinoflagellate cyst records were observed during this time interval in the Santa Barbara Basin and

on the California margin, where SST and PP were qualitatively and quantitatively reconstructed by Pospelova et al. (2006, 2015).

Despite the low PP indicated by both marine organic carbon from Chang et al. (2008) and dinoflagellate cyst concentrations in this study, heterotrophic taxa were more than ten times as abundant as autotrophic taxa, as shown by the H/A ratios (Fig. 2). The highest PCA1 scores in Zone I (prior to 11.6 cal kyr BP) were positively correlated with *Brigantedinium* taxa (Fig. 3a). High abundances of *Brigantedinium* spp. have been associated with increased nutrients due to regional upwelling or river input (e.g., Bringue et al., 2013, 2014; Li et al., 2018, 2020; Pospelova et al., 2006, 2008, 2010; Price and Pospelova, 2011; Radi and de Vernal, 2008). However, in our record, predominant *Brigantedinium* taxa in assemblages occurred in an environment with weaker upwelling and likely nutrient-poor meltwater input at the site. This was likely also associated with original cyst sources and depositional conditions influenced by glacial meltwater, as discussed previously. During this time interval, it is possible that more cysts came from the shelf areas near Barkley Sound and the mouth of the Strait of Juan de Fuca, compared to time intervals without major meltwater inputs. Particularly, a large volume of glacial meltwater coming through the Strait of Juan de Fuca could have flowed northwestward into the ocean, potentially enhancing cross-shelf transport and carrying more surface cysts from the shelf areas where *Brigantedinium* species might be dominant. More details of dinoflagellate cyst assemblages on the shelf during this time interval are worth investigating in future studies. Contrarily, tropical regions, such as the South China Sea (Li et al., 2021) and the Gulf of California (Price et al., 2013), that have larger riverine sediment inputs but were not influenced by ice sheets during this time interval showed a different response. At these locations, the terrestrial materials were nutrient-rich and promoted much higher

cyst production than in the Holocene, mainly contributed by *Brigantedinium* spp. (e.g., Li et al., 2017, 2021).

In addition, RDA results show that the abundances of *Brigantedinium* spp., *Brigantedinium simplex*, *Lejeunecysta sabrina*, cysts of *Polykrikos schwartzii*, *Quinquecuspis concreta*, and cysts of *Pentapharsodinium dalei*, were positively correlated with Mn/Al ratios but negatively with Mo concentrations and Mo/Al ratios (Fig. 3b). In core MD02-2496, these redox proxies suggest that pore waters within the surface sediments remained oxygenated due to lower overall PP and less decay of exported organic matter (e.g., Chang et al., 2008, 2014). Cysts of *Pentapharsodinium dalei* have been observed in cooler waters (e.g., Dale, 1996; Zonneveld et al., 2013). Thus, the first axes of PCA and RDA could explain the presence of cyst assemblages with cooler waters, greater terrestrial input, possibly weaker upwelling, and more oxygenated surface sediments before 11.6 cal kyr BP on the Vancouver Island margin.

5.3. Changes in oceanographic conditions and marine PP during the Holocene

5.3.1. ~11.6-10.6 cal kyr BP (Zone II)

After ~11.6 cal kyr BP, the depositional environment on the Vancouver Island margin is characterized by a fourfold reduction in the proportion of sand and a consistent input of finer sediments (<63 μm) (Fig. 4n), as the CIS continued to retreat from the coast. By ~10.6 cal kyr BP, $\delta^{15}N_{bulk}$ showed the highest enrichment to 8–9‰ (Fig. 4f), and concentrations of marine organic carbon (Fig. 4e) and Mo (Fig. 4g) increased greatly, suggesting reduced terrestrial input, invigorated upwelling of nutrient-rich waters, enhanced export production, and increased oxygen demand (suboxic conditions) in the upper sediment column (Chang et al., 2008, 2014). Both relative and absolute abundances of *Nematosphaeropsis labyrinthus* reached their highest in Zone II (Fig. 4m). High abundances of this species were also observed on the California Margin and in

the Gulf of California from ~12 to 10 cal kyr BP (Price et al., 2013; Pospelova et al., 2015). A rapid increase in *N. labyrinthus* was also recorded in the eastern North Atlantic at the beginning of the Holocene, with the highest value at ~11 cal kyr BP (e.g., Harland et al., 2016). *Nematosphaeropsis labyrinthus* is commonly found with higher percentages in offshore locations, and the relative abundances of this species are positively correlated with distance away from the coastlines (e.g., Dale, 1996; de Vernal et al., 2020; Pospelova et al., 2008; Zonneveld et al., 2013). A few exceptions observed that *Nematosphaeropsis labyrinthus* could be restricted to a fully marine environment, e.g., the deep basin of the South China Sea (Li et al., 2020) and offshore of the western United States (Pospelova et al., 2008), but could also be found in isolated phosphorus-limited lagoonal settings (Pospelova et al., 2004). In open-marine environments, *Nematosphaeropsis labyrinthus* is typically accompanied by *Impagidinium* species (e.g., Li et al., 2020; Pospelova et al., 2008; Zonneveld et al., 2013). In this study, the abundances of *N. labyrinthus* during this time interval increased together with *Operculodinium centrocarpum* sensu Wall and Dale 1966, whereas the highest abundances of *Impagidinium* species occurred immediately afterwards. This pattern suggests a shift from coastal-oceanic boundary conditions (e.g., Dale and Dale, 2002) to more oceanic influence as glacial meltwater inputs decreased in Zone II.

Reconstruction of SSTs off Vancouver Island showed the warmest sea surface temperature (~12°C) appearing at ~10.7 cal kyr BP (Fig. 5d), that was likely related to a maximum in summer solar insolation at 50°N (e.g., Kienast and McKay, 2001). Enhanced PP at ~10.6 cal kyr BP is corroborated by total cyst concentrations, which were 2–7 times higher than in Zone I (Figs. 2 and 4b). Autotrophic dinoflagellates saw a major increase, with a first peak in relative abundances contributed mainly by opportunistic *Operculodinium centrocarpum* sensu Wall and Dale 1966,

which has been observed year-round in coastal British Columbia (e.g., Pospelova et al., 2010; Price and Pospelova, 2011; Radi et al., 2007; Radi and de Vernal, 2004).

5.3.2. ~10.6-8.2 cal kyr BP (Subzones IIIa and IIIb)

Fluctuating total cyst concentrations and significant shifts in dominant species within cyst assemblages indicate possible instability in the marine ecosystem during 10.6–8.2 cal kyr BP. In this period, the highest total cyst concentrations occurred (Fig. 4b), with autotrophic taxa replacing heterotrophic taxa as the main contributors (Fig. 4i). Most heterotrophic taxa decreased in relative abundance (Fig. 2a), and *Operculodinium centrocarpum* sensu Wall and Dale 1966 replaced *Brigantedinium* species (Fig. 4d) as the predominant species in the assemblages (Fig. 4j), with a shift towards the truncate-process type dominating in 9–8.2 cal kyr BP (Fig. 4k). Abundances of *Spiniferites* species increased (Fig. 4l), and *Impagidinium* taxa appeared and reached their highest abundances, along with *Hiddenocysta matsuokae*, whereas *Nematosphaeropsis labyrinthus* almost disappeared from the record (Fig. 4m). The highest autotrophic taxa abundances (Fig. 4i), primarily contributed by *Operculodinium centrocarpum* sensu Wall and Dale 1966 (Fig. 4j) and *Spiniferites* species (Fig. 4l), were likely affected by climatic changes such as intensified insolation, corresponding to the highest intensity of summer solar insolation at 50°N (Fig. 4h). This warm condition, coupled with abundant nutrients (i.e., $\delta^{15}N_{bulk}$), is reflected in the negative scores of RDA axis 1 and positive scores of RDA axis 2 for these taxa (Fig. 3b). However, the appearance of *Impagidinium* taxa, dominated by *Impagidinium aculeatum* (Fig. 2), indicates the presence of oceanic water masses over the coring site, as *Impagidinium* species are commonly found in oligotrophic, open-ocean environments (e.g., Dale et al., 2002; Li et al., 2017, 2021; Pospelova et al., 2008; Radi and de Vernal, 2004; Zonneveld and Pospelova, 2015; Zonneveld et al., 2013).

Cysts of *Hiddenocysta matsuokae* exhibited the highest abundance in Subzone IIIa. This species was first identified by Gurdebeke et al. (2021) from the sediments collected from estuaries in British Columbia (Kyuquot Sound in western Vancouver Island and Hidden Basin on the mainland coast). The presence of *Hiddenocysta matsuokae* in MD02-2496 suggests that the motile stage potentially flourished not only in shallow estuaries but also in deeper ocean environments. Interestingly, in a sediment core from Kyuquot Sound (Gurdebeke et al., 2021), *Hiddenocysta matsuokae* had a similar maximum abundance during the same time interval as in MD02-2496 (Gurdebeke et al., 2021). This observation may indicate more productive marine waters in southwestern British Columbia, favorable to *Hiddenocysta matsuokae*, during this time of increased solar insolation (Fig. 4h) and generally warmer SST (Fig. 5j).

The notably high abundances of *Operculodinium centrocarpum*-truncate processes during 9.0–8.2 cal kyr BP (Subzone IIIb) could have been induced by a short-term cooling event that also resulted in a general decline in PP (Figs. 4b and 4e). A lower marine primary productivity (PP) and a minor cooling during a similar time interval (~9 – ~7 cal kyr BP) were also inferred from dinoflagellate cyst records on the California margin (Pespolova et al., 2015). The process length of *Operculodinium centrocarpum*-truncate processes was reported to be significantly positively correlated with salinity and temperature in the Northern Hemisphere (e.g., Mertens et al., 2011, 2012a; Jansson et al., 2014; Willumsen et al., 2013), as well as with sea-surface water density (e.g., Bringue et al., 2016; Mertens et al., 2012b; Verleye et al. 2012). Thus, the high abundance of *Operculodinium centrocarpum*–truncate processes in our study could reflect low SST, sea-surface density, or salinity during 9.0–8.2 cal kyr BP. This record likely corresponds to the 8.2 ka cooling event, an abrupt and widespread climate instability characterized by dry, dusty conditions, a dramatic increase in forest fire frequency, and rapid cooling in the Northern Hemisphere (e.g.,

519 Adhikari et al., 2002; Alley et al., 1997; Wang et al., 2005; Song et al., 2017, 2023). The 8.2 ka
520 event was triggered by the outflow of lakes Agassiz and Ojibway into the Labrador Sea, resulting
521 in disruption of the Atlantic meridional overturning circulation (e.g., Barber et al., 1999; Morrill
522 et al., 2012). However, Rohling and Palike (2005) argued the 8.2 ka event is part of a climate
523 deterioration at ~8.5–8.0 cal kyr BP that was related to solar output fluctuations. From lacustrine
524 sediment records in southwestern British Columbia, Walker and Pellatt (2003) reported peak
525 summer temperatures and minimum precipitation in the period of 9–7 cal kyr BP, with winter
526 temperatures colder than today. Comparably, in our study, the onset of the rapid increase in
527 abundance of *Operculodinium centrocarpum*–truncate processes also occurred at ~9.0 cal kyr BP
528 and ended almost as abruptly at ~8.2 cal kyr BP. This limited event may be related to a combination
529 of climate deterioration - cooler winters and dryer summers, and a deceleration of sea-level rise
530 that followed a rapid sea-level rise induced by short-term events (e.g., Meltwater Pulse1B) due to
531 glacial isostatic adjustment (Fig. 4a; Dallimore et al., 2008; Friele and Hutchinson, 1993; Harrison
532 et al., 2019; Kendall et al., 2008; Lambeck et al., 2014). Deceleration of sea-level rise resulted in
533 the deposition of terrestrial materials closer to the coast, e.g. worldwide initiation of Holocene
534 marine deltas (Stanley and Wrne, 1994), and led to decreased transport of the materials into deeper
535 marine environments. Thus, the flourishing of *Operculodinium centrocarpum*-truncate processes
536 and the rapid decline of PP during this time interval might also be influenced by this process
537 besides the climate change. The terrestrial materials in the Holocene might have more nutrients
538 because waters flew through multi-bioecosystems on land, comparing with nutrient-poor terrestrial
539 materials during the Pleistocene, which mainly transported by meltwaters from ice-eroded
540 bedrocks or ice-grounded sediments. It is worth conducting a detailed study on how a sudden

reduction in terrestrial material could affect dinoflagellates and their cyst assemblages on the continental slope.

5.3.3. ~8.2-6.5 cal kyr BP (Subzone IVa)

Total cyst concentrations suggest that PP stayed at a relatively low level following the 8.2 ka event until 6.5 cal kyr BP (Zone IVa), after which it slightly increased again (Fig. 4b). The decline of *Impagidinium* species, with only occasional appearances in the middle-late Holocene, inferred weakened influences from ocean currents such as California current or California Undercurrent, well consistent with the continuing depletion in $\delta^{15}N_{bulk}$ in MD02-2496 (Fig. 4f; Chang et al., 2008) and lower SST reconstructed from nearby core JT96-09PC (Fig. 5d) as Kienast and McKay (2001).

Based on our PCA results (Fig. 3a), the samples from 8.2 to 6.5 cal kyr BP were mainly separated from others by the negative scores of PCA1 axis, which were correlated with autotrophic *Operculodinium centrocarpum* sensu Wall and Dale 1966, *Spiniferites* spp., and *Spiniferites ramosus*. The RDA results revealed significant correlations of these taxa with TOC, TN, $\delta^{13}C_{org}$, and Mo/Al ratios (Fig. 3b). Chang et al. (2008) suggested that organic carbon originated through biological fixation in the euphotic zone aka phytoplankton blooms, while sedimentary Mo enrichments were generated at the seafloor in response to increased oxidant demand, indicating sedimentary anoxia.

5.3.4. After ~6.5 cal kyr BP (subzones IVb and IVc)

Most samples younger than 6.5 cal kyr BP had negative scores along PCA2 axis and were positively correlated with cysts of Diplopsalid, *Echinidinium aculeatum*, *Echinidinium* spp., *Islandinium pacificum*, and cysts of *Protoperidinium* spp. The RDA results showed that Ba concentration was a statistically significant parameter, along with TOC, TN, and $\delta^{13}C_{org}$ (Fig. 3b).

Ba occurs in marine barite, which is associated with siliceous debris (i.e., diatoms) and decaying particulate organic matter in the water column (e.g., Paytan and Griffith, 2007). As primary consumers of diatoms, heterotrophic dinoflagellates, and their cysts, often occur in high abundance during diatom blooms (e.g., Sherr and Sherr, 2007; Bringue et al., 2013; Pospelova et al., 2010; Price and Pospelova, 2011). Therefore, in our study, the positive correlation between heterotrophic cysts and Ba concentration suggests intensified upwelling conditions that were conducive to diatom blooms, which reflects and therefore an overall increase in marine PP during this time.

After ~4.0 cal kyr BP (Subzone IVc), PP appears to be relatively stable with only a slight decrease, consistent with the trend in sedimentary TOC (Fig. 4b, e). Abundances of autotrophic taxa and *Brigantedinium* remained relatively stable, whereas changes in other heterotrophic taxa were notable. For instance, increases in both relative abundances and concentrations of cysts of *Diplopsalid*, *Dubridinium cavatum*, *Echinidinium* spp., *Islandinium pacificum*, cysts of *Protoperidinium* spp., *Selenopemphix undulata*, and total *Votadinium* mainly contributed to the increase in heterotrophic taxa, which gradually prevailed over the autotrophic taxa in abundances. *Echinidinium aculeatum* and other undetermined RBSCs increased in the late Holocene after ~4 cal kyr BP (IVc). Decreases in total cyst concentrations at ~3.5 cal kyr BP, along with an increase in abundances of heterotrophic undetermined RBSCs, possibly corresponded to lower upwelling intensity and warmer SSTs in the northeastern Pacific (e.g., Bringue et al., 2013, 2014; Pospelova et al., 2006, 2015) and low insolation at ~3.5 cal kyr BP as reported by Patterson et al. (2004).

5.4. Comparison with other regions along the western North America margin

Studies on paleoceanography and marine paleoproductivity in the late Quaternary have been conducted on several sediment cores collected from the continental shelf, slope, and ocean basins along the western North America margin (e.g., Addison et al., 2018; Barron et al., 2003,

2022; Chang et al., 2008; Friddell et al., 2003; Kienast and McKay, 2001; Lyle et al., 2001; McGann, 2011; McKay et al., 2004; Palmer et al., 2023; Pisias et al., 2001; Pospelova et al., 2006, 2015; Seki et al., 2002). Synthesizing reconstructed SST records from the California Current System, in various locations off the west coast of the United States, Palmer et al. (2023) found that cold conditions during the latest Pleistocene ended at the onset of warming in the early Holocene, which was followed by the return of cool SSTs during the mid-Holocene, then again by warmer SSTs in the Late Holocene.

Generally, PP along the western North American margin was low in the latest Pleistocene and high in the Holocene (Figs. 5a–c, f, g, l, and n), as reflected by the records in sediments from MD02-2496 (this study; Chang et al., 2008), JT96-09PC (Kienast and McKay, 2001), ODP-1019 (Barron et al., 2003), TN062-0550 (Addison et al., 2018), EW9504-13PC (Pisias et al., 2001), JPC-76 (Friddell et al., 2003), ODP-1017E (Pospelova et al., 2015), and ODP-893A (Pospelova et al., 2006). This pattern corresponds well to climate warming from the Pleistocene to the Holocene, as indicated by *n*-alkenone-derived SSTs (Figs. 5d, e, j, and k), as well as by cyst assemblage data (Pospelova et al., 2015). Kienast and McKay (2001) interpreted that the rapid SST change off Vancouver Island was controlled by the atmospheric transmission of the climate signal from the North Atlantic.

However, the fluctuations of both PP and SST varied spatiotemporally along the western North American margin. Before ~11 cal kyr BP, PP showed only slight changes in the north (Figs. 5a–c) and was more variable towards the south (Figs. 5f, g, and m). In contrast, SST during this time interval fluctuated greatly, with the B-A and Younger Dryas events well-defined in the north (Figs. 5d, e) and more subtle toward the south (Figs. 5j and k). The observed latitudinal differences in PP and SSTs may be due to the influence of cooled meltwater and nutrient-poor coarse

sediments delivered by meltwater or outbursts, which was proximal to the northern locations. Delivery of glacial meltwater in the north muted the PP signal, suppressing upwelling and/or diluting nutrients and amplifying the SST signal directly through cold meltwater input. However, cold water influencing the south was through net Northern Hemisphere cooling when the climate changed, as founded by Praetorius et al. (2020) that cooled and freshened meltwater had significant impacts on changes in ocean circulation using a numerical model to simulate the flow trajectory of Columbia River megafloods (46.25˚N) in the late Pleistocene and the Holocene.

At ~10.6 cal kyr BP, export production, indicated by TOC, increased rapidly and dinoflagellate cysts reached their highest abundances, which was triggered by a possible combination of strengthened solar insolation, increased denitrification in the ETNP and/or increased strength of the California Undercurrent, and invigorated coastal upwelling. After this time, the increase in total export production slowed down or stayed relatively stable as shown by the organic carbon. However, multiple proxies of the surface ecosystem showed different trends prior to 6.5 cal kyr BP. Siliceous microplankton (e.g., diatoms) decreased off southern Oregon (Fig. 5f; Barron et al., 2003), whereas dinoflagellate cyst abundances showed a rapid decrease followed by a gradual increase off Vancouver Island (Fig. 5a; this study), along the upwelling margin of southern California (Fig. 5l; Pospelova et al., 2015), and in Santa Barbara Basin (Fig. n; Pospelova et al., 2006). Between ~10.6 and 6.5 cal kyr BP, SSTs gradually declined in northern locations but increased in southern locations. An intensified influence of the California Undercurrent along the coast may have pushed the California Current farther away from the Vancouver Island margin and strengthened the Davidson Current. This may have resulted in cooling surface waters and reducing water column stratification in the north, which may not have occurred off southern California (Pospelova et al., 2015). Overall, these changes were likely

triggered by changes in insolation, which suppressed wind stress in the spring and enhanced wind stress in the summer and autumn in the California Current System (Diffenbaugh and Ashfaq, 2007), thereby amplifing changes in seasonal SSTs. In addition, the 8.2 ka cooling event was not uniformly recorded across all locations along the western North American margin. However, likely the related events were reflected by dinoflagellate cysts from 9.0 to 8.2 cal kyr BP off Vancouver Island and from 9.0 to 7.0 cal kyr BP off southern California (Fig. 4k). Oster et al. (2017) reconstructed more frequent or intense winter storms on the California coast during the 8.2 ka event, although the magnitude of change was not as pronounced as those in the high northern latitudes and monsoon-influenced areas of the north Pacific Ocean.

During 6.5–4.0 cal kyr BP, PP was relatively stable along the Vancouver Island margin (Figs. 5a–d). SSTs were likely stabilized but slightly lower than those during the intervals of 10.6-6.5 cal kyr BP and 4.0-2.3 cal kyr BP (Figs. 5d, e, j, k). The lower temperatures were also reflected by the higher values of $\delta^{18}O$ (Fig. 5 m; Friddell et al., 2003). Testing the sensitivity of wind-driven upwelling in the California Current to mid-Holocene orbital forcing at 6 cal kyr BP, Diffenbaugh et al. (2003) explained that a cooler hydroclimate could be related to a longer and less vigorous upwelling season, with a decreased seasonal contrast, which could explain the lower PP in the south.

6. Conclusions

This study presents the first dinoflagellate cyst record spanning the Late Pleistocene to the Holocene (~14 to ~2.3 cal kyr BP) on the Vancouver Island margin. We identified 40 cyst taxa, including 14 produced by autotrophic and 26 by heterotrophic dinoflagellate taxa. Four dinoflagellate cyst zones and five subzones were defined.

Dinoflagellate cyst Zone I was characterized by *Brigantedinium* species in the cyst assemblages, the lowest total cyst concentrations, and the highest H/A values. Combining these records with marine geochemical records from Chang et al. (2008, 2014) and the history of general ice retreat, low PP and strong effects from glacial meltwater input to the coast were indicative of environmental conditions from 14–11.6 cal kyr BP. The nutrient-poor meltwater and cooler climate did not result in high PP.

Zone II represented the first thousand years of the Holocene (11.6 – 10.6 cal kyr BP) and was dominated by the highest abundances of *Nematosphaeropsis labyrinthus*. A gradual increase in the concentrations of total cysts and organic carbon during this time suggest that PP increased gradually as well. A notable increase in the abundances of autotrophic taxa, dominated by *Operculodinium centrocarpum* sensu Wall and Dale 1966, and a decrease in heterotrophic taxa were observed, resulting in a decreasing trend in H/A ratios. The strong presence of *N. labyrinthus* was interpreted to represent an environment of coastal and oceanic boundary conditions.

Zone III, spanning from ~10.6 to ~8.2 cal kyr BP, was characterized by the highest abundances of autotrophic taxa and the lowest abundances of heterotrophic taxa, resulting in the lowest H/A values. The cyst assemblages were dominated by the autotrophic *Operculodinium centrocarpum* sensu Wall and Dale 1966. PP was much higher, even doubled or tripled, than in Zone II as reflected by the concentrations of total cyst and organic carbon. The highest abundances of *Impagidinium* taxa indicated a more oceanic influence.

Cyst assemblages of Subzone IIIa (~10.6–9.0 cal kyr BP) were dominated by *Operculodinium centrocarpum* sensu Wall and Dale, whereas Subzone IIIb (~9.0 – ~8.2 cal kyr BP) saw *Operculodinium centrocarpum*-truncate processes become the more abundant taxon. We interpret the high abundance of *O. centrocarpum*-truncate processes to indicate a specific event on

678 the Vancouver Island margin that involved. This includes rapid sea-level rise, intensified seasonal
679 influence of the California Undercurrent, and possible climate change, such as the cooling 8.2 ka
680 event.

681 Zone IV (~8.2 to ~2.3 cal kyr BP) was characterized by similar relative abundances of
682 autotrophic and heterotrophic cyst taxa. In general, the abundances of *Brigantedinium* spp. and
683 *Brigantedinium simplex* remained relatively stable throughout Zone IV, whereas *Dubridinium*
684 *cavatum*, *Echinidinium* spp., cysts of Diplopsalid, and *Islandinium pacificum* increased. The
685 subzones were defined by subtle differences in the cyst assemblages. A gradual increase in
686 autotrophic taxa defined Subzone IVa (~8.2 – ~6.5 cal kyr BP), followed by an increase in
687 heterotrophic taxa in Subzone IVb (~6.5 –~4.0 cal kyr BP), and culminating in heterotrophic
688 dominance in Subzone IVc (~4 –2.3 cal kyr BP). Subzone IVa had the lowest total cyst
689 concentrations in the Holocene but the highest abundances of *Spiniferites*. Subzone IVb (~6.5 –
690 ~4.0 cal kyr BP) was characterized by relatively stable total cyst concentrations and the highest
691 abundances of *Islandinium pacificum*, *Selenopemphix undulata*, and *Votadinium spinosum*.
692 Subzone IVc (~4 to ~2.3 cal kyr BP) saw total cyst concentrations decrease but the appearance of
693 the highest abundances of *Echinidinium aculeatum* and a rapid increase in undetermined RBSCs.

694 We compared our results with previously published reconstructions of climatic and
695 oceanographic conditions along western North America and identified spatiotemporal variations
696 in PP and SSTs. Before ~11 cal kyr BP, fluctuations in PP appeared to be greater off the coast of
697 California than on the Vancouver Island margin, while fluctuations in SSTs showed a reverse
698 pattern between these southern and northern locations. This pattern was likely associated with the
699 proximal impacts of cool and nutrient-poor meltwater from the retreating CIS on the Vancouver
700 Island margin, which were absent in the southern regions.

Between ~10.6 and ~6.5 cal kyr BP, organic carbon indicated total export production increased across the regions along western North America. However, PP was characterized by a rapid decline and then a gradual increase after reaching the peak at ~10.6 cal kyr BP, reflected by dinoflagellate cyst concentrations. This trend could be associated with the relative impacts of the California Undercurrent and the intensity or duration of coastal upwelling, mainly triggered by changes in insolation. SSTs exhibited a decline in the northern regions and an increase in the southern regions could be explained that changes in insolation may have affected wind stresses and resultant coastal upwelling more in the north than in the south. In addition, the 8.2 ka event was not uniformly recorded across all locations along the western North American margin. The possible expression of this event in our record, occurring from 9.0 to 8.2 cal kyr BP likely resulted from a combination of climate change and decelerated sea-level rise.

Both PP and SSTs were relatively stable from ~6.5 to ~4.0 cal kyr BP along the western North American coast. However, while PP sustained high levels, SSTs were lower compared to time intervals before and after this time interval. This cooler interval might reflect a prolonged and less vigorous upwelling season and decreased temperature contrasts between seasons.

Acknowledgments

This work was funded by the Natural Sciences and Engineering Research Council of Canada (NSERC) to Dr. Z. Li through a Postdoctoral Fellowship (PDF–516186–2018). We are very grateful to Dr. T. S. Hamilton at the Geological Survey of Canada for his suggestions on the geological background of the study area, and to M. Soon for her assistance during the subsampling of core MD02-2496 at the University of British Columbia.

Author Contributions

V. Pospelova and Z. Li designed the study and the methods. Z. Li performed subsampling at UBC, and sample preparation and dinoflagellate cyst analysis at UBC and the University of Minnesota. A. Chang provided the sedimentary geochemical data. V. Pospelova and K. Mertens assisted with cyst identification. Y. Wu provided oceanographic modeling interpretations. Z. Li drafted the manuscript with input from all co-authors, who contributed to writing, editing and revisions.

References

Addison, J.A., Barron, J., Finney, B., Kusler, J., Bukry, D., Heusser, L.E., Alexander, C.R., 2018. A Holocene record of ocean productivity and upwelling from the northern California continental slope. Quaternary International 469, 96–108. doi:10.1016/j.quaint.2017.02.021

Adhikari, D.P., Kumon, F., Kawajiri, K., 2002. Holocene climate variability as deduced from the organic carbon and diatom records in the sediments of Lake Aoki, central Japan. Journal of the Geological Society of Japan 108, 249–265. doi: 10.5575/geosoc.108.249

Alley, R.B., Mayewski, P.A., Sowers, T., Stuiver, M., Taylor, K.C., Clark, P.U., 1997. Holocene climatic instability: A prominent, widespread event 8200 yr ago. Geology 25, 483–486. doi:10.1130/0091-7613(1997)025 <0483:HCIAPW>2.3.CO;2

Anderson, D.M., Lively, J.J., Reardon, E.M., Price, C.A., 1985. Sinking characteristics of dinoflagellate cysts. Limnology and Oceanography 30, 1000–1009. doi:10.4319/lo.1985.30.5.1000.

Antoine, D., Jean-Michel, A., Morel, A., 1996. Ocean primary production 2. Estimation at global scale from satellite (Coastal Zone Colour Scanner) chlorophyll. Global Biogeochemical Cycles 10, 57–69. doi:10.1029/95GB02832

745 Barber, D.C., Dyke, A., Hillaire-Marcel, C., Jennings, A.E., Andrews, J.T., Kerwin, M.W.,
746 Bilodeau, G., McNeely, R., Southon, J., Morehead, M.D., Gagnon, J.M., 1999. Forcing of
747 the cold event of 8,200 years ago by catastrophic drainage of Laurentide lakes. Nature 400,
748 344–348. doi:10.1038/22504
749 Barron, J.A., Heusser, L., Herbert, T., Lyle, M., 2003. High-resolution climatic evolution of coastal
750 northern California during the past 16,000 years. Paleoceanography 18, 1020.
751 doi:10.1029/2002PA000768
752 Barron, J.A., Bukry, D., 2007. Development of the California Current during the past 12,000 yr
753 based on diatoms and silicoflagellates. Palaeogeography, Palaeoclimatology,
754 Palaeoecology 248, 313–338. doi:10.1029/2002PA000800
755 Barron, J.A., Addison, J.A., Heusser, L.E., Bukry, D., Schwartz, V., Wagner, A., 2022. An 11,300
756 yr record of paleoclimatology and paleoceanography of the central California coast in a
757 gravity core from Pioneer Seamount. Quaternary International 621, 74–83.
758 doi:10.1016/j.quaint.2019.12.019
759 Behl, R.J., Kennett, J.P., 1996. Brief interstadial events in the Santa Barbara basin, NE Pacific,
760 during the past 60 kyr. Nature 379, 243–246.
761 Bringué, M., Pospelova, V., Pak, D., 2013. Seasonal production of organic-walled dinoflagellate
762 cysts in an upwelling system: A sediment trap study from the Santa Barbara Basin,
763 California. Marine Micropaleontology 100, 34–51. doi:10.1016/j.marmicro.2013.03.007
764 Bringué, M., Pospelova, V. Field, D.B., 2014. High resolution sedimentary record of dinoflagellate
765 cysts reflects decadal variability and 20th century warming in the Santa Barbara
766 Basin. Quaternary Science Reviews 105, 86–101. doi:10.1016/j.quascirev.2014.09.022

767 Bringué, M., Pospelova, V., Calvert, S.E., Enkin, R.J., Lacourse, T., Ivanochko, T., 2016. High
768 resolution dinoflagellate cyst record of environmental change in Effingham Inlet (British
769 Columbia, Canada) over the last millennium. Palaeogeography, Palaeoclimatology,
770 Palaeoecology 441, 787–810. doi:10.1016/j.palaeo.2015.10.026
771 Calvert, S.E., Pedersen, T.F., 1992. Organic carbon accumulation and preservation in marine
772 sediments: How important is anoxia? In Whelan, J.K., Farrington, J.W. (Eds.), Organic
773 Matter: Productivity, Accumulation and Preservation in Recent and Ancient Sediments
774 (pp. 231–263). Columbia University Press.
775 Calvert, S.E., Pedersen, T.F., 1996. Sedimentary geochemistry of manganese: Implications for the
776 environment of formation of manganiferous black shales. Economic Geology 91, 36–47.
777 doi:10.2113/gsecongeo.91.1.36
778 Chang, A.S., Pedersen, T.F., Hendy, I.L., 2008. Late Quaternary paleoproductivity history on the
779 Vancouver Island margin, western Canada: a multiproxy geochemical study. Canadian
780 Journal of Earth Sciences 45, 1283–1297. doi:10.1139/E08-038
781 Chang, A.S., Pedersen, T.F., Hendy, I.L., 2014. Effects of productivity, glaciation, and ventilation
782 on late Quaternary sedimentary redox and trace element accumulation on the Vancouver
783 Island margin, western Canada. Paleoceanography 29, 730–746.
784 doi:10.1002/2013PA002581
785 Clague, J.J., 1981. Late Quaternary geology and geochronology of British Columbia. Part 2:
786 Summary and discussion of radiocarbon dated Quaternary history. Geological Survey of
787 Canada, Paper 80–35, 41pp.
788 Clague, J.J., James, T.S., 2002. History and isostatic effects of the last ice sheet in southern British
789 Columbia. Quaternary Science Review 21, 71–87. doi:10.1016/S0277-3791(01)00070-1

790 Cosma, T., Hendy, I.L., 2008. Pleistocene glacimarine sedimentation on the continental slope off
791 Vancouver Island, British Columbia. Marine Geology 255, 45–54.
792 doi:10.1016/j.margeo.2008.07.001
793 Cosma, T.N., Hendy, I.L., Chang, A.S., 2008. Chronological constraints on Cordilleran Ice Sheet
794 glaciomarine sedimentation from core MD02-2496 off Vancouver Island (western
795 Canada). Quaternary Science Review, 27941–955. doi:10.1016/j.quascirev.2008.01.013
796 Crawford, W.R., Thomson, R.E., 1991. Physical oceanography of the western Canadian
797 continental shelf. Continental Shelf Research 11, 669–683. doi:10.1016/0278-
798 4343(91)90073-F
799 Cummins, P.F., Freeland, H.J., 2007. Variability of the North Pacific Current and its bifurcation.
800 Progress in Oceanography 75, 253–265. doi:10.1016/j.pocean.2007.08.006
801 Dale, B., 1976. Cyst formation, sedimentation, and preservation: factors affecting dinoflagellate
802 assemblages in recent sediments from Trondheimsfjord, Norway. Review of Palaeobotany
803 and Palynology 22, 39-60. doi:10.1016/0034-6667(76)90010-5
804 Dale, B., 1996. Dinoflagellate cyst ecology: modeling and geological applications. In Jansonius
805 and McGregor (Eds.), Palynology: Principles and Applications (pp. 1249–1275). AASP
806 Foundation.
807 Dale, B., Dale, A., 2002. Environmental applications of dinoflagellate cysts and
808 acritarchsS. Haslett (Ed.), Quaternary Environmental Micropaleontology, Edward Arnold
809 Lda, London (2002), pp. 207–240.
810 Dale, B., Dale, A.L., Jansen, J.H.F., 2002. Dinoflagellate cysts as environmental indicators in
811 surface sediments from the Congo deep-sea fan and adjacent regions. Palaeogeography,
812 Palaeoclimatology, Palaeoecology 185, 309–338. doi:10.1016/S0031-0182(02)00380-2

Dethier, D.P., Pessl, J.F., Keuler, R.F., Balzarini, M.A., Pevear, D.R., 1995. Late Wisconsinan glaciomarine deposition and isostatic rebound, northern Puget Lowland, Washington. Geological Society of America Bulletin 107, 1288–1303. doi:10.1130/0016-7606(1995)107<1288:LWGDAI>2.3.CO;2

de Vernal, A., Henry, M., Matthiessen, J., Mudie, P.J., Rochon, A., Boessenkool, K.P., Eynaud, F., Grosfjeld, K., Guiot, J., Hamel, D., Harland, R., Head, M.J., Kunz-Pirrung, M., Levac, E., Loucheur, V., Peyron, O., Pospelova, V., Radi, T., Turon, J.L., Voronina, E., 2001. Dinoflagellate cyst assemblages as tracers of sea-surface conditions in the northern North Atlantic, Arctic and sub-Arctic seas: the new 'n=677' database and its application for quantitative palaeoceanographic reconstruction. Journal of Quaternary Science 16, 681–698. doi:10.1002/jqs.659

de Vernal, A., Radi, T., Zaragosi, S., Van Nieuwenhove, N., Rochon, A., Allan, E., De Schepper, S., Eynaud, F., Head, M.J., Limoges, A., Londeix, L., Marret, F., Matthiessen, J., Penaud, A., Pospelova, V., Price, A., Richerol, T., 2020. Distribution of common modern dinoflagellate cyst taxa in surface sediments of the Northern Hemisphere in relation to environmental parameters: the new n = 1968 database. Marine Micropaleontology, 101796. doi:10.1016/j.marmicro.2019.101796.

Diffenbaugh, N.S., Ashfaq, M., 2007. Response of California Current forcing to mid-Holocene insolation and sea surface temperatures: wind forcing of the California Current. Paleoceanography 22, PA3101. doi:10.1029/2006PA001382

Diffenbaugh, N.S., Sloan, L.C., Snyder, M.A., 2003. Orbital suppression of wind-driven upwelling in the California Current at 6 ka. Paleoceanography 18, 1051. doi:10.1029/2002pa000865

Dallimore, A., Enkin, R.J., Pienitz, R., Southon, J.R., Baker, J., Wright, C.A., Pedersen, T.F., Calvert, S.E., Ivanochko, T., Thomson, R.E., 2008. Postglacial evolution of a Pacific coastal fjord in British Columbia, Canada: interactions of sea-level change, crustal response, and environmental fluctuations-results from MONA core MD02-2494. *Canadian* Journal of Earth Sciences 45, 1345–1362. doi:10.1139/E08-042

Esper, O., Zonneveld, K., 2002. Distribution of organic-walled dinoflagellate cysts in surface sediments of the Southern Ocean (eastern Atlantic sector) between the subtropical front and the Weddell Gyre. Marine Micropaleontology 46, 177–208. doi:10.1016/S0377-8398(02)00041-5

Fisler, J., Hendy, I.L., 2008. California Current System response to late Holocene climate cooling in southern California. Geophysical Research Letters 35, L09702. doi:10.1029/2008GL033902

Friddell, J.E., Thunell, B.C., Guilderson, T.P., Kashgarian, M., 2003. Increased northeast Pacific climatic variability during the warm middle Holocene. Geophysical Research Letters 30, 14-1–14-3. doi:10.1029/2002GL016834

Friele, P.A., Hutchinson, I., 1993. Holocene sea-level change on the central west coast of Vancouver Island, British Columbia. Canadian Journal of Earth Sciences 30, 832–840. doi:10.1139/e93-069

Grimm, E.C., 1991. Tilia-Graph Program. Illinois State Museum, Springfield, IL.

Grimm, E.C., 1992. Tilia Program. Illinois State Museum, Springfield, IL.

Gurdebeke, P.R., Pospelova, V., Mertens, K.N., Dallimore, A., Chana, J., Louwye, S., 2018. Diversity and distribution of dinoflagellate cysts in surface sediments from fjords of

western Vancouver Island (British Columbia, Canada. Marine Micropaleontology 143, 12–29. doi:10.1016/j.marmicro.2018.07.005

Gurdebeke, P.R., Mertens, K.N., Pospelova, V., Matsuoka, K., Li, Z., Gribble, K.E., Gu, H., Bogus, K., Vrielinck, H., Louwye, S., 2020a. Taxonomic revision, phylogeny, and cyst wall composition of the dinoflagellate cyst genus *Votadinium* Reid (Dinophyceae, Peridiniales, Protoperidiniaceae). Palynology 44, 310–335. doi:10.1080/01916122.2019.1580627

Gurdebeke, P.R., Mertens, K.N., Pospelova, V., Nieuwenhove, N.V., Louwy, S., 2020b. *Islandinium pacificum* sp. nov., a new dinoflagellate cyst from the upper Quaternary of the northeast Pacific. Palynology 44, 80–93. doi:10.1080/01916122.2018.1549118

Gurdebeke, P.R., Mertens, K.N., Meyvisch, P., Bogus, K., Pospelova, V., Louwy, S., 2021. *Hiddenocysta matsuokae* gen. et sp. nov. from the Holocene of Vancouver Island, British Columbia, Canada. Palynology 45, 103–114. doi:10.1080/01916122.2020.1750500

Harland, R., Asteman, I.P., Morley, A, Morris, A., Harris, A, Howe, J.A., 2016. Latest Quaternary palaeoceanographic change in the eastern North Atlantic based upon a dinoflagellate cyst event ecostratigraphy. Heliyon 2, e00114. doi:10.1016/j.heliyon.2016.e00114

Harrison, S., Smith, D.E., Glasser, N.F., 2019. Late Quaternary meltwater pulses and sea level change. Journal of Quaternary Science 1–15. doi:10.1002/jqs.3070

Hendy, I.L., Cosma, T., 2008. Vulnerability of the Cordilleran Ice Sheet to iceberg calving during late Quaternary rapid climate change events. Paleoceanography 23, PA2101. doi:10.1029/2008PA001606

878 Hewitt, A., Mosher, D.C., 2001. Late Quaternary stratigraphy and seafloor geology of eastern Juan
879 de Fuca Strait, British Columbia and Washington. Marine Geology 177, 295–316. doi:
880 10.1016/S0025-3227(01)00160-8
881 Hickey, B.M., Banas, N.S., 2008. Why is the northern end of the California Current System so
882 productive? Oceanography 21(4), 90–107. doi.org/10.5670/oceanog.2008.07
883 Hickey, B.M., McCabe, R., Geier, S., Dever, E., Kachel, N., 2008. Three interacting freshwater
884 plumes in the northern California Current System. Journal of Geophysical Research 114,
885 C00B03. doi:10.1029/2008JC004907
886 Hughen, K.A., Baillie, M.G.L., Bard, E., Beck, J.W., Bertrand, C.J.H., Blackwell, P.G., Buck,
887 C.E., Burr, G.S., Cutler, K.B., Damon, P.E., Edwards, R.L., Fairbanks, R.G., Friedrich, M.,
888 Guilderson, T.P., Kromer, B., McCormac, G., Manning, S., Ramsey, C.B., Reimer, P.J.,
889 Reimer, R.W., Remmele, S., Southon, J.R., Stuiver, M., Talamo, S., Taylor, F.W., van der
890 Plicht, J., Weyhenmeyer, C.E., 2004. Marine04 marine radiocarbon age calibration, 0–26
891 cal kyr BP. Radiocarbon 46 (3), 1059–1086. doi:10.1017/S0033822200033002
892 Jansson, I.M., Mertens, K.N., Head, M.J., 2014. Statistically assessing the correlation between
893 salinity and morphology in cysts produced by the dinoflagellate Protoceratium reticulatum
894 from surface sediments of the North Atlantic Ocean, Mediterranean–Marmara–Black Sea
895 region, and Baltic–Kattegat–Skagerrak estuarine system. Palaeogeography,
896 Palaeoclimatology, Palaeoecology 399, 202–213. doi:10.1016/j.palaeo.2014.01.012
897 Kendall, R.A., Mitrovica, J.X., Milne, G.A., Törnqvist, T.E., Li, Y., 2008. The sea-level fingerprint
898 of the 8.2 ka climate event. Geology 36, 423–426. doi:10.1130/G24550A.1

899 Kienast, S.S., McKay, J.L., 2001. Sea surface temperatures in the subarctic northeast Pacific reflect
900 millennial-scale climate oscillations during the last 16 kyrs. Geophysical Research Letters
901 28, 1563–1566. doi:10.1029/2000GL012543
902 Krassovski, M., 1993. Investigation of the California Undercurrent off the West Coast of
903 Vancouver Island (Master's thesis). Moscow State University, 59 pp.
904 Kung, R., Douglas, K., Stacey, C.D., 2023. Canada west coast topo-bathymetric digital elevation
905 model, British Columbia; Geological Survey of Canada, Open File 8963 (ver. 2021), 80 p.
906 doi:10.4095/331539
907 Lambeck, K., Rouby, H., Purcell, A., Sun, Y., Sambridge, M., 2014. Sea level and global ice
908 volumes from the Last Glacial Maximum to the Holocene. Proceedings of the National
909 Academy of Sciences of the United States of America 111, 15296–15303.
910 doi:10.1073/pnas.1411762111
911 Lewis, J., Dodge, J.D., Powell, A.J., 1990. Quaternary dinoflagellate cysts from the upwelling
912 system offshore Peru, hole 686B, ODP Leg 112. Proceedings of the Ocean Drilling
913 Program, Scientific Results 112, 323–328. 10.2973/odp.proc.sr.112.162.1990
914 Li, Z., Pospelova, V., Liu, L.J., Zhou, R., Song, B., 2017. High-resolution palynological record of
915 Holocene climatic and oceanographic changes in the northern South China Sea.
916 Palaeogeography, Palaeoclimatology, Palaeoecology 483, 94–124.
917 doi:10.1016/j.palaeo.2017.03.009
918 Li, Z., Pospelova, V., Lin, H.-L., Liu, L., Song, B., 2018. Seasonal dinoflagellate cyst production
919 and terrestrial palynomorph deposition in the monsoon influenced South China Sea: a
920 sediment trap study from the Southwest Taiwan waters. Review of Palaeobotany and
921 Palynology 257, 117–139. doi:10.1016/j.revpalbo.2018.07.007

Li, Z., Pospelova, V., Kawamura, H., Luo, C., Mertens, K.N., Hernández-Almeida, I., Yin, K., Wu, Y., Wu, H., Xiang, R., 2020. Dinoflagellate cyst distribution in surface sediments from the South China Sea in relation to hydrographic conditions and primary productivity. Marine Micropaleontology, 101815. doi:10.1016/j.marmicro.2019.101815.

Li, Z., Pospelova, V., Liu, L., Francois, R., Wu, Y., Mertens, K.N., Saito, Y., Zhou, R., Song, B., Xie, X., 2021. High-resolution reconstructions of Holocene sea-surface conditions from dinoflagellate cyst assemblages in the northern South China Sea. Marine Geology 438, 106528. doi:10.1016/j.margeo.2021.106528.

Li, Z., Pospelova, V., Mertens, K.N., Liu, L., Wu, Y., Li, C., Gu, H., 2023. Evaluation of organic-walled dinoflagellate cyst distributions in coastal surface sediments of the China Seas in relation with hydrographic conditions for paleoceanographic reconstruction. Quaternary International 661, 60–75. doi:10.1016/j.quaint.2023.03.007

Limoges, A., de Vernal, A., Van Nieuwenhove, N., 2014. Long-term hydrological changes in the northeastern Gulf of Mexico (ODP-625B) during the Holocene and late Pleistocene inferred from organic-walled dinoflagellate cysts. Palaeogeography, Palaeoclimatology, Palaeoecology 414, 178–191. doi:10.1016/j.palaeo.2014.08.019

Lyle, M., Heusser, L., Herbert, T., Mix, A., 2001. Interglacial theme and variations: 500 k.y. of orbital forcing and associated responses from the terrestrial and marine biosphere, U.S. Pacific Northwest. Geology 29, 1115–1118. doi:10.1130/0091-7613(2001)029<1115:ITAVKY>2.0.CO;2

Mackas, D.L., Denman, K.L., Bennett, A.F., 1987. Least squares multiple tracer analysis of water mass composition. Journal of Geophysical Research 92, 2907–2918. doi:10.1029/JC092iC03p02907

945 Marret, F., Zonneveld, K.A.F., 2003. Atlas of organic-walled dinoflagellate cyst distribution.
946 Review of Palaeobotany and Palynology 125, 1–200. doi:10.1016/S0034-6667(02)00229-
947 4
948 Marret, F., de Vernal, A., McDonald, D., Pedersen, T., 2001. Middle Pleistocene to Holocene
949 palynostratigraphy of ODP Site 887 in the Gulf of Alaska, northeast North Pacific.
950 Canadian Journal of Earth Sciences 38, 373–386. doi:10.1139/e00-092
951 Mathewes, R.W., 1993. Evidence for Younger Dryas-age cooling on the North Pacific coast of
952 America. Quaternary Science Reviews 12, 1993, 321-331. doi:10.1016/0277-
953 3791(93)90040-S
954 Matsuoka, K., 1988. Cyst-theca relationships in the diplopsalid group (Peridiniales, Dinophyceae).
955 Review of Palaeobotany and Palynology 56, 95–122. doi:10.1016/0034-6667(88)90077-2
956 Matsuoka, K., Kawami, H., Nagai, S., Iwataki, M., Takayama, H., 2009. Re-Examination of cyst-
957 motile relationships of Polykrikos kofoidii Chatton and Polykrikos schwartzii Butschli
958 (Gymnodiniales, Dinophyceae). Review of Palaeobotany and Palynology 154, 79–90.
959 doi:10.1016/j.revpalbo.2008.12.013
960 McGann, M., 2011. Paleoceanographic changes on the Farallon Escarpment off central California
961 during the last 16,000 years. Quaternary International 235, 26–39.
962 doi:10.1016/j.quaint.2010.09.005.
963 McGann, M., 2015. Correlation of marine and coastal terrestrial records of central California:
964 Response to paleoceanographic and paleoclimatic change during the past 19,000 years.
965 Quaternary International 387, 58–71. doi:10.1016/j.quaint.2015.01.037

966 McKay, J.L., Pedersen, T.F., Kienast, S.S., 2004. Organic carbon accumulation over the last 16
967 kyr off Vancouver Island, Canada: Evidence for increased marine productivity during the
968 deglacial. Quaternary Science Reviews 23, 261–281. doi:10.1016/j.quascirev.2003.07.004.
969 McKay, J.L., Pedersen, T.F., Southon, J., 2005. Intensification of the oxygen minimum zone in
970 the northeast Pacific off Vancouver Island during the last deglaciation: Ventilation and/or
971 export production? Paleoceanography 20, PA4002. doi:10.1029/2003PA000979.
972 Mertens, K.N., Dale, B., Ellegaard, M., Jansson, I.-M., Godhe, A., Kremp, A., Louwye, S., 2011.
973 Process length variation in cysts of the dinoflagellate Protoceratium reticulatum, from
974 surface sediments of the Baltic–Kattegat–Skagerrak estuarine system: a regional salinity
975 proxy. Boreas 40, 242–255. doi:10.1111/j.1502-3885.2010.00193.
976 Mertens, K.N., Bradley, L.R., Takano, Y., Mudie, P.J., Marret, F., Aksu, A.E., Hiscott, R.N.,
977 Verleye, T.J., Mousing, E.A., Smyrnova, L.L., Bagheri, S., Mansor, M., Pospelova, V.,
978 Matsuoka, K., 2012a. Quantitative estimation of Holocene surface salinity variation in the
979 Black Sea using dinoflagellate cyst process length. Quaternary Science Reviews 39, 45–
980 59. doi:10.1016/j.quascirev.2012.01.026
981 Mertens, K.N., Bringue´, M., Nieuwenhove, N.V., Takano, Y., Pospelova, V., Rochon, A., De
982 Vernal, A., Radi, T., Dale, B., Patterson, R.T., Weckstrom, K., Andren, E., Louwye, S.,
983 Matsuoka, K., 2012b. Process length variation of the cyst of the dinoflagellate
984 Protoceratium reticulatum in the North Pacific and Baltic-Skagerrak region: calibration as
985 an annual density proxy and first evidence of pseudo-cryptic speciation. Journal of
986 Quaternary Science 27, 734–744. doi:10.1002/jqs.2564
987 Mertens, K.N., Gu, H.F., Gurdebeke, P.R., Takano, Y., Clarke, D., Aydin, H., Li, Z., Pospelova,
988 V., Shin, H.H., Li, Z., Matsuoka, K., Head, M.J., 2020. A review of rare, poorly known,

and morphologically problematic extant marine organic-walled dinoflagellate cyst taxa of the orders Gymnodiniales and Peridiniales from the Northern Hemisphere. Marine Micropaleontology 159, 101773. doi:10.1016/j.marmicro.2019.101773

Morrill, C., LeGrande, A.N., Renssen, H., Bakker, P., Otto-Bliesner, B.L., 2012. Model sensitivity to North Atlantic freshwater forcing at 8.2 ka. Climate of the Past Discussions 8, 3949–3976. doi:10.5194/cpd-8-3949-2012.

Mudie, P.J., Rochon, A., Levac, E., 2002. Palynological records of red tide-producing species in Canada: past trends and implications for the future. Palaeogeography, Palaeoclimatology, Palaeoecology 180, 159–186. doi:10.1016/S0031-0182(01)00427-8

Nooteboom, P.D., Bijl, P.K., Sebille, E., Heydt, A.S., Dijkstra, H.A., 2019. Transport bias by ocean currents in sedimentary microplankton assemblages: Implications for paleoceanographic reconstructions. Paleoceanography and Paleoclimatology 34, 1178–1194. doi:10.1029/2019PA003606.

Ohfuchi, W., Nakamura, H., Yoshioka, M.K., Enomoto, T., Takaya, K., Peng, X., Yamane, S., Nishimura, T., Kurihara, Y., Ninomiya, K., 2004. 10-km mesh meso-scale resolving simulations of the global atmosphere on the Earth Simulator: Preliminary outcomes of AFES (AGCM for the Earth Simulator). Journal of the Earth Simulator 1, 8–34. doi:10.32131/jes.1.8

Oster, J.L., Sharp, W.D., Covey, A.K., Gibson, J., Rogers, B., Mix, H., 2017. Climate response to the 8.2 ka event in coastal California. Scientific Reports 7, 3886. doi:10.1038/s41598-017-04215-5.

1010 Over, J.S., Pospelova, V., 2022. Last Interglacial (MIS 5e) sea surface hydrographic conditions in
1011 coastal southern California based on dinoflagellate cysts. Palaeogeography,
1012 Palaeoclimatology, Palaeoecology 591, 110875. Doi:10.1016/j.palaeo.2022.110875
1013 Palmer, H.M., Vriesman, V.P., Livsey, C.M., Fish, C.R., Hill, T.M., 2023. Holocene climate and
1014 oceanography of the coastal Western United States and California Current System. Climate
1015 of the Past,19, 199–232. doi:10.5194/cp-19-199-2023
1016 Patterson, R.T., Prokoph, A., Chang, A., 2004. Late Holocene sedimentary response to solar and
1017 cosmic ray activity influenced climate variability in the NE Pacific. Sedimentary Geology
1018 172, 67–84. doi:10.1016/j.sedgeo.2004.07.007.
1019 Patterson, R.T., Swindles, G.T., Roe, H.M., Kumar, A., Prokoph, A., 2011. Dinoflagellate cyst-
1020 based reconstructions of mid to late Holocene winter sea-surface temperature and
1021 productivity from an anoxic fjord in the NE Pacific Ocean. Quaternary International 235
1022 (1–2), 13–25. doi:10.1016/j.quaint.2010.06.016
1023 Paytan, A., Griffith, E.M., 2007. Marine barite: Recorder of variations in ocean export
1024 productivity. Deep Sea Research Part II: Topical Studies in Oceanography 54, 687–705.
1025 doi:10.1016/j.dsr.2007.01.007.
1026 Pisias, N.G., Mix, A.C., Heusser, L., 2001. Millennial scale climate variability of the northeast
1027 Pacific Ocean and northwest North America based on radiolaria and pollen. Quaternary
1028 Science Reviews, 20, 1561–1576. doi:10.1016/S0277-3791(01)00018-X
1029 Pospelova, V., Kim, S.-J., 2010. Dinoflagellate cysts in recent estuarine sediments from
1030 aquaculture sites of southern South Korea. Marine Micropaleontology 76, 37–51.
1031 https://doi.org/10.1016/j.marmicro.2010.04.003

1032 Pospelova, V., Chmura, G.L., Walker, H.A., 2004. Environmental factors influencing the spatial
1033 distribution of dinoflagellate cyst assemblages in shallow lagoons of southern New
1034 England (USA). Review of Palaeobotany and Palynology 128, 7–34. doi:10.1016/S0034-
1035 6667(03)00110-6
1036 Pospelova, V., Chmura, G.L., Boothman, W.S., Latimer, J.S., 2005. Spatial distribution of modern
1037 dinoflagellate cysts in polluted estuarine sediments from Buzzards Bay (Massachusetts,
1038 USA) embayments. Marine Ecology Progress Series 292, 23–40. doi:10.3354/meps292023
1039 Pospelova, V., Pedersen, T.F., de Vernal, A., 2006. Dinoflagellate cysts as indicators of climatic
1040 and oceanographic changes during the past 40 kyr in the Santa Barbara Basin, southern
1041 California. Paleoceanograph, 21, PA2010. doi:10.1029/2005PA001251.
1042 Pospelova, V., de Vernal, A., Pedersen, T.F., 2008. Distribution of dinoflagellate cysts in surface
1043 sediments from the northeastern Pacific (43-25°N) in relation to sea-surface conditions and
1044 upwelling. Marine Micropaleontology 68(1–2), 21–48.
1045 doi:10.1016/j.marmicro.2008.01.008.
1046 Pospelova, V., Esenkulova, S., Johannessen, S.C., O'Brien, M.C., Macdonald, R.W., 2010.
1047 Organic-walled dinoflagellate cyst production, composition and flux from 1996 to 1998 in
1048 the central Strait of Georgia (BC, Canada): a sediment trap study. Marine
1049 Micropaleontology 75, 17–37. doi:10.1016/j.marmicro.2010.02.003
1050 Pospelova, V., Price, A.M., Pedersen, T.F., 2015. Palynological evidence for late Quaternary
1051 climate and marine primary productivity changes along the California margin.
1052 Paleoceanography 30, 877–894. doi:10.1002/2014PA002728

1053 Praetorius, S.K., Condron, A., Mix, A.C., Walczak, M.H., McKay, J.L., Du, J., 2020. The role of
1054 Northeast Pacific meltwater events in deglacial climate change. *Science Advances* 6,
1055 eaay2915. doi:10.1126/sciadv.aay2915
1056 Price, A.M., Pospelova, V., 2011. High-resolution sediment trap study of organic-walled
1057 dinoflagellate cyst production and biogenic silica flux in Saanich Inlet (BC, Canada).
1058 Marine Micropaleontology 80, 18-43. doi:10.1016/j.marmicro.2011.03.003
1059 Price, A.M., Mertens, K.N., Pospelova, V., Pedersen, T.F., Ganeshram, R.S., 2013. Late
1060 Quaternary climatic and oceanographic changes in the Northeast Pacific as recorded by
1061 dinoflagellate cysts from Guaymas Basin, Gulf of California (Mexico). Paleoceanography
1062 28 200–212. doi:10.1002/palo.20019.
1063 Radi, T., de Vernal, A., 2004. Dinocyst distribution in surface sediments from the northeastern
1064 Pacific margin (40–60°N) in relation to hydrographic conditions, productivity and
1065 upwelling. Review of Palaeobotany and Palynology 128, 169–193. doi:10.1016/S0034-
1066 6667(03)00118-0
1067 Radi, T., de Vernal, A., 2008. Dinocysts as proxy of primary productivity in mid-high latitudes of
1068 the Northern Hemisphere. Marine Micropaleontology 68, 84–114.
1069 doi:10.1016/j.marmicro.2008.01.012
1070 Radi, T., Pospelova, V., de Vernal, A., Barrie, J.V., 2007. Dinoflagellate cysts as indicators of
1071 water quality and productivity in British Columbia estuarine environments. Marine
1072 Micropaleontology 62, 269–297. doi:10.1016/j.marmicro.2006.09.002
1073 Reed, R.K., Halpern, D., 1976. Observations of the California Undercurrent off Washington and
1074 Vancouver Island. Limnology and Oceanography 21, 389–398.
1075 doi:10.4319/lo.1976.21.3.0389

1076 Reimer, P.J., Baillie, M.G.L., Bard, E., Bayliss, A., Beck, J.W., Bertrand, C.J.H., Blackwell, P.G.,
1077 Buck, C.E., Burr, G.S., Cutler, K.B., Damon, P.E., Edwards, R.L., Fairbanks, R.G.,
1078 Friedrich, M., Guilderson, T.P., Hogg, A.G., Hughen, K.A., Kromer, B., McCormac, G.,
1079 Manning, S., Ramsey, C.B., Reimer, R.W., Remmele, S., Southon, J.R., Stuiver, M.,
1080 Talamo, S., Taylor, F.W., van der Plicht, J., Weyhenmeyer, C.E., 2004. IntCal04 terrestrial
1081 radiocarbon age calibration, 0–26 cal kyr BP. Radiocarbon 46 (3), 1029–1058.
1082 doi:10.1017/S0033822200032999
1083 Rochon, A., de Vernal, A., Sejrup, H.P., Haflidason, H., 1998. Palynological evidence of climatic
1084 and oceanographic changes in the North Sea during the last deglaciation. Quaternary
1085 Research 49, 197–207. doi:10.1006/qres.1997.1956
1086 Rochon, A., de Vernal, A., Turon, J.L., Matthiessen, J., Head, M.J., 1999. Distribution of recent
1087 dinoflagellate cysts in surface sediments from the North Atlantic Ocean and adjacent seas
1088 in relation to sea-surface conditions. Review of Palaeobotany and Palynology 105, 1–52.
1089 doi:10.1016/j.jmarsys.2007.11.003
1090 Rohling, E.J., Palike, H., 2005. Centennial-scale climate cooling with a sudden cold event around
1091 8200 years ago. Nature 434, 975–979. Doi:10.1038/nature03421
1092 Sasaki, H., Nonaka, M., Masumoto, Y., Sasai, Y., Uehara, H., Sakuma, H., 2008. An eddy-
1093 resolving hindcast simulation of the quasi-global ocean from 1950 to 2003 on the Earth
1094 Simulator. In: Hamilton, K., Ohfuchi, W., Eds.), High Resolution Numerical Modelling of
1095 the Atmosphere and Ocean. Springer, New York, NY, 157–186. doi:10.1007/978-0-387-
1096 49791-4_10.

1097 Seki, O., Ishiwatari, R., Matsumoto, K., 2002. Millennial climate oscillations in NE Pacific surface
1098 waters over the last 82 kyr: New evidence from alkenones. Geophysical Research Letters
1099 29, 2144. doi:10.1029/2002GL015200.
1100 Sherr, E.B., Sherr, B.F., 2007. Heterotrophic dinoflagellates: a significant component of
1101 microzooplankton biomass and major grazers of diatoms in the sea. Marine Ecology
1102 Progress Series 352, 187–197. doi:10.3354/meps07161
1103 Stanley, D.J., Warne, A.G., 1994. Worldwide initiation of Holocene marine deltas by deceleration
1104 of sea-level rise. Science 265, 228–31. doi:10.1126/science.265.5169.228
1105 Song, B., Li, Z., Lu, H., Mao, L., Saito, Y., Yi, S., Lim, J., Li, Z., Lu, A., Sha, L., Zhou, R., Zuo,
1106 X., Pospelova, V., 2017. Pollen record of the centennial climate changes during 9–7 cal ka
1107 BP in the Changjiang (Yangtze) River Delta plain, China. Quaternary Research 87, 275–
1108 287. doi:10.1016/j.palaeo.2022.111335
1109 Song, B., Li, Z., Mao, L., Saito, Y., Yang, X., Yang, S., 2023. Vegetation succession, climate
1110 change and cold events during 9.2–8.0 cal kyr BP in eastern China: High-resolution pollen
1111 evidence from the Yangtze delta plain area. Palaeogeography, Palaeoclimatology,
1112 Palaeoecology 610, 111335. doi:10.1016/j.palaeo.2022.111335
1113 Stuiver, M., Reimer, P.J., Reimer, R.W., 2004. CALIB 4.0. Available online at www.calib.org.
1114 Taylor, M.A., Hendy, I.L., Pak, D.K., 2014. Deglacial ocean warming and marine margin retreat
1115 of the Cordilleran Ice Sheet in the North Pacific Ocean. Earth and Planetary Science Letters
1116 403, 89–98. doi:10.1016/j.epsl.2014.06.026
1117 Ter Braak, C.J.F., Smilauer, P., 2012. Canoco Reference Manual and User's Guide: Software for
1118 Ordination (Version 5). Microcomputer Power, Ithaca, NY, USA, p. 496.

Thomson, R.E., 1981. Oceanography of the British Columbia Coast. Canadian Special Publication of Fisheries and Aquatic Sciences 56, 29 pp.

Thomson, R.E., Krassovski, M.V., 2010. Poleward reach of the California Undercurrent extension. Journal of Geophysical Research 115, C09027. doi:10.1029/2010JC006280.

Walker, I.R., Pellatt, M.G., 2003. Climate change in coastal British Columbia—A paleoenvironmental perspective. Canadian Water Resources Journal 28, 531–566. doi:10.4296/cwrj2804531

Wang, Y., Cheng, H., Edwards, R.L., He, Y., Kong, X., An, Z., Wu, J., Kelly, M.J., Dykoski, C. A., Li, X., 2005. The Holocene Asian monsoon: Links to solar changes and North Atlantic climate. Science 308, 854–857. doi:10.1126/science.1106296

Ware, D.M., Thomson, R.E., 2005. Bottom-up ecosystem trophic dynamics determine fish production in the Northeast Pacific. Science 308, 1280–1284. doi:10.1126/science.1109049

Willumsen, P.S., Filipsson, H.L., Reinholdsson, M., Lenz, C., 2013. Surface salinity and nutrient variations during the Littorina Stage in the Fårö Deep, Baltic Sea. Boreas 42, 210–223. doi:10.1111/j.1502-3885.2012.00286.x

Van Nieuwenhove, N., Head, M.J., Limoges, A., Pospelova, V., Mertens, K.N., Matthiessen, J., De Schepper, S., de Vernal, A., Eynaud, F., Londeix, L., Marret, F., Penaud, A., Radi, T., Rochon, A., 2020. An overview and brief description of common marine organic-walled dinoflagellate cyst taxa occurring in surface sediments of the Northern Hemisphere. Marine Micropaleontology 159, 101814. doi:10.1016/j.marmicro.2019.101814

Verleye, T.J., Louwye, S., 2010. Late Quaternary environmental changes and latitudinal shifts of the Antarctic Circumpolar Current as recorded by dinoflagellate cysts from offshore Chile (41°S). Quaternary Science Reviews 29, 1025–1039. doi:10.1016/j.quascirev.2010.01.009

Verleye, T.J., Mertens, K.N., Young, M.D., Dale, B., McMinn, A., Scott, L., Zonneveld, K.A.F., Louwye, S., 2012. Average process length variation of the marine dinoflagellate cyst *Operculodinium centrocarpum* in the tropical and Southern Hemisphere Oceans: assessing its potential as a palaeosalinity proxy. Marine Micropaleontology 86–87, 45–58. doi:10.1016/j.marmicro.2012.02.001

Zonneveld, K.A.F., Pospelova, V., 2015. A determination key for modern dinoflagellate cysts. Palynology 39, 387–409. doi:10.1080/01916122.2014.990115

Zonneveld, K.A.F., Marret, F., Versteegh, G.J.M., Bogus, K., Bonnet, S., Bouimetarhan, I., Crouch, E., de Vernal, A., Elshanawany, R., Edwards, L., Esper, O., Forke, S., Grosfjeld, K., Henry, M., Holzwarth, U., Kielt, J.F., Kim, S.Y., Ladouceur, S., Ledu, D., Chen, L., Limoges, A., Londeix, L., Lu, S.H., Mahmoud, M.S., Marino, G., Matsouka, K., Matthiessen, J., Mildenhal, D.C., Mudie, P., Neil, H.L., Pospelova, V., Qi, Y., Radi, T., Richerol, T., Rochon, A., Sangiorgi, F., Solignac, S., Turon, J.L., Verleye, T., Wang, Y., Wang, Z., Young, M., 2013. Atlas of modern dinoflagellate cyst distribution based on 2405 data points. Review of Palaeobotany and Palynology 191, 1–197. doi:10.1016/j.revpalbo.2012.08.003

Zonneveld, K.A.F., Grotheer, H., Versteegh, G.J.M., 2022. Dinoflagellate cysts production, excystment and transport in the upwelling off Cape Blanc (NW Africa). Frontiers in Marine Science 9, doi:10.3389/fmars.2022.915755.

Tables and figures

Table 1. List of dinoflagellate cyst taxa identified in this study.

Fig. 1. Bathymetric map with prevailing wind directions and currents in winter and summer, extensions of glacier margins (Clague and James, 2002), and the location of sediment core MD02-2496 used in this study (a). The regional ocean currents and the sites of comparison cores are shown in the inset map (b). The green circles in (a) are the potential sites where dinoflagellates cysts originated in surface waters before they started to sink, based on an online particle trace simulation tool (planktondrift.science.uu.nl; Nooteboom et al., 2019). CIS: Cordilleran Ice Sheet. LIS: Laurentide Ice Sheet.

Fig. 2. Abundances of total cysts, autotrophic (in dark blue) and heterotrophic (in green) taxa, as well as selected (>1%) individual dinoflagellate cyst taxa, heterotrophic to autotrophic (H/A) ratios, principal components analysis (PCA1 and PCA2) scores, dinoflagellate cyst zones, and sediment fractions. Relative abundances (%) are shown in (a), while concentrations (cysts g^{-1}) are depicted in (b). The horizontal solid and dashed lines across the figure delineate dinoflagellate cyst zones and subzones (I to IVc) marked in color bars. Zonation is determined by constrained cluster analysis (CONISS) of relative abundances of dinoflagellate cysts. Calibrated ages from Cosma et al. (2008). Sediment fraction data are from Cosma & Hendy (2008).

Fig. 3. Ordination diagrams generated by (a) principal components analysis (PCA) and (b) redundancy analysis (RDA) for dinoflagellate cyst relative abundances in core MD02-2496. The colored circles correspond to samples from the same-colored dinoflagellate cyst zones and subzones shown in Fig. 2a. The environmental parameters in (b) are significant with *p*-values <0.05. Geochemical and organic isotope data are from Chang et al. (2008, 2014). Al: aluminum, Ba: barium, Mo: molybdenum, Mn: manganese, TN: total nitrogen, TOC: total organic carbon.

Stable isotope ratios for $d^{13}C_{org}$ were measured from organic carbon in sediments; $d^{15}N_{bulk}$ values were measured from bulk sediments.

Fig. 4. Dinoflagellate cyst records (b-d and i-m; marked with asterisks; this study) and geochemical records (e-g; Chang et al., 2008) in core MD02-2496, corresponding to changes in (a) Relative sea level (Fiele and Hutchinson, 1993; Dallimore et al., 2008), (h) Summer solar insolation (Walker and Pellatt, 2003), (n) Sedimentary environment indicated by (n) coarse (>63 mm) sediment fraction (MD02-2496; Cosma and Hendy, 2008), and (o) ice retreat (Clague and James, 2002), with (p) Paleoenvironment and palaeoceanographic interpretations. The gray bars mark notable short-term changes in the dinoflagellate cyst records. The red bar highlights the highest insolation and relative abundances of autotrophic taxa. The dark blue bars highlight more oceanic conditions with less meltwater influence after complete ice sheet retreat from Vancouver Island. The light blue bar denotes the presence of extensive ice caps. B-A: Bølling-Allerød. YD: Younger Dryas. MWP1B: Meltwater Pulse 1B. 8.2: 8.2 ka event. Zones: dinoflagellate cyst zones from this study.

Fig. 5. Regional comparison of proxies for marine productivity and reconstructed SSTs from sediment cores along the western North American margin. Core locations are illustrated in Fig. 1a. (a) Total dinoflagellate cyst concentrations (MD02-2496; This study); (b) Marine and total organic carbon (MD02-2496; Chang et al., 2008); (c) Marine organic carbon (JT96-09PC; McKay et al., 2004); (d) Sea-surface temperature (JT96-09PC; Kienast and McKay, 2001); (e) Sea-surface temperature, (f) opal, and (g) total organic carbon (ODP-1019; Barron et al., 2003); (h) $\delta^{13}C_{org}$ and (i) opal (TN062-0550; Addison et al., 2018); (j) Sea-surface temperature (EW9504-13PC; Pisias et al., 2001); (k) Sea-surface temperature (ODP-1017E; Seki et al., 2002); (l) Total dinoflagellate cyst concentrations (ODP-1017E; Pospelova et al., 2015); (m) Planktonic foraminiferal

Globigerina bulloides $\delta^{18}O$ (JPC-76; Friddell et al., 2003); and (n) Total dinoflagellate cyst concentrations (ODP-893A; Pospelova et al., 2006). The gray bars indicate intervals of relatively stable dinoflagellate cyst concentrations from core MD02-2496. The black arrows denote intervals of notable trending of changes in each proxy.

Plate I. 1. *Impagidinium aculeatum*, UMN17-265. 2. *Impagidinium paradoxum*, UMN17-265. 3. *Impagidinium strialatum*, UMN17-292. 4. *Impagidinium pallidum*, UMN17-292. 5. *Nematosphaeropsis labyrinthus*, UMN17-222. 6. *Operculodinium centrocarpum* sensu Wall and Dale 1966, UMN17-208. 7. *Operculodinium centrocarpum* -truncate processes, UMN17-208. 8–9. Cysts of *Pentapharsodinium dalei*, UMN17-212. 10–11. *Hiddenocysta matsuokae*, UMN17-263. Scale bars are 10 μm.

Plate II. 1. *Spiniferites ramosus*, UMN17-290. 2. *Spiniferites* sp. 1, UMN17-206. 3. *Spiniferites* spp., UMN17-290. 4–5. *Spiniferites elongatus*, 4: UMN17-265; 5: UMN17-292. 6. *Brigantedinium cariacoense*, UMN17-204. 7. *Brigantedinium irregulare*, UMN17-227. 8–9. *Brigantedinium simplex*, 8: UMN17-202; 9: UMN17-261. 10–11. Cysts of Diplopsalid, 10: UMN17-204; 11: UMN17-198. 12–13. *Dubridinium cavatum*, 12: UMN17-250; 13: UMN17-300. Scale bars are 10 μm.

Plate III. 1. *Echinidinium aculeatum*, UMN17-216. 2–3. *Echinidinium* spp., 2: UMN17-222; 3: UMN17-202. 4–5. *Islandinium pacificum*, 4: UMN17-208; 5: UMN17-206. 6. Cyst of *Polykrikos kofoidii*, UMN17-204. 7. Cyst of *Polykrikos schwartzii*, UMN17-265. 8–9. *Lejeunecysta sabrina*, UMN17-261. 10–13. *Lejeunecysta* spp., 10: UMN17-263; 11: UMN17-204; 12, 13: UMN17-198. 14. *Leipokatium invisitatum*, UMN17-250. 15. *Quinquecuspis concreta*, UMN17-292. Scale bars are 10 μm.

Plate IV. 1–4. *Quinquecuspis concreta*, 1, 2: UMN17-208; 3: UMN17-239; 4: UMN17-304. 5. Cyst of *Protoperidinium* sp. 1, UMN17-292. 6. *Selenopemphix nephroides*, UMN17-204. 7. *Selenopemphix undulata*, UMN17-250. 8. *Selenopemphix quanta*, UMN17-204. 9–11. *Votadinium calvum*, 9: UMN17-250; 10: UMN17-208; 11: UMN17-261. 12–13. *Votadinium pontifossatum*, 12: UMN17-204; 13: UMN17-292. 14. *Votadinium spinosum*, UMN17-265. 15–16. Undetermined cysts, 15: UMN17-204; 16: UMN17-263. Scale bars are 10 μm.

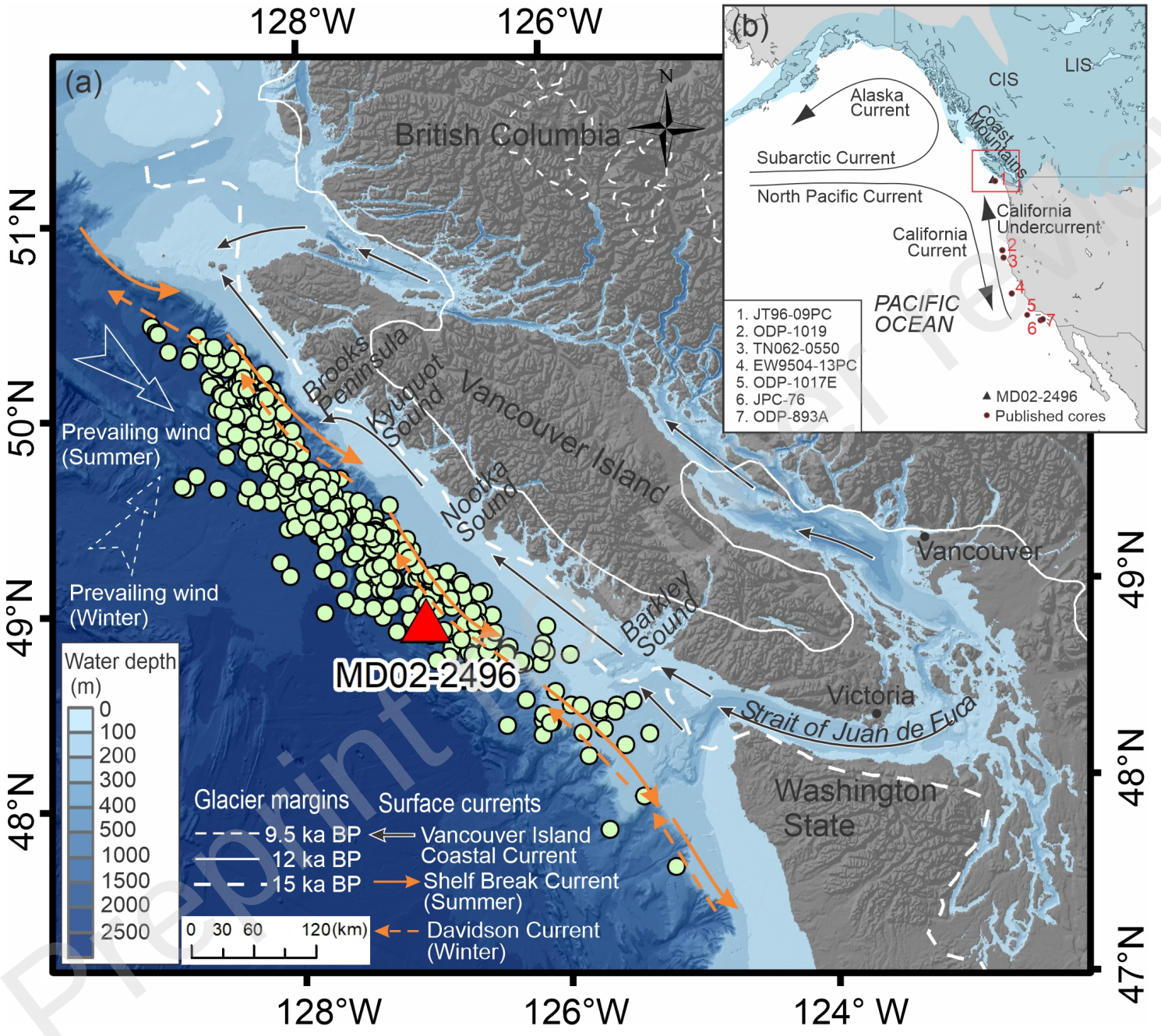

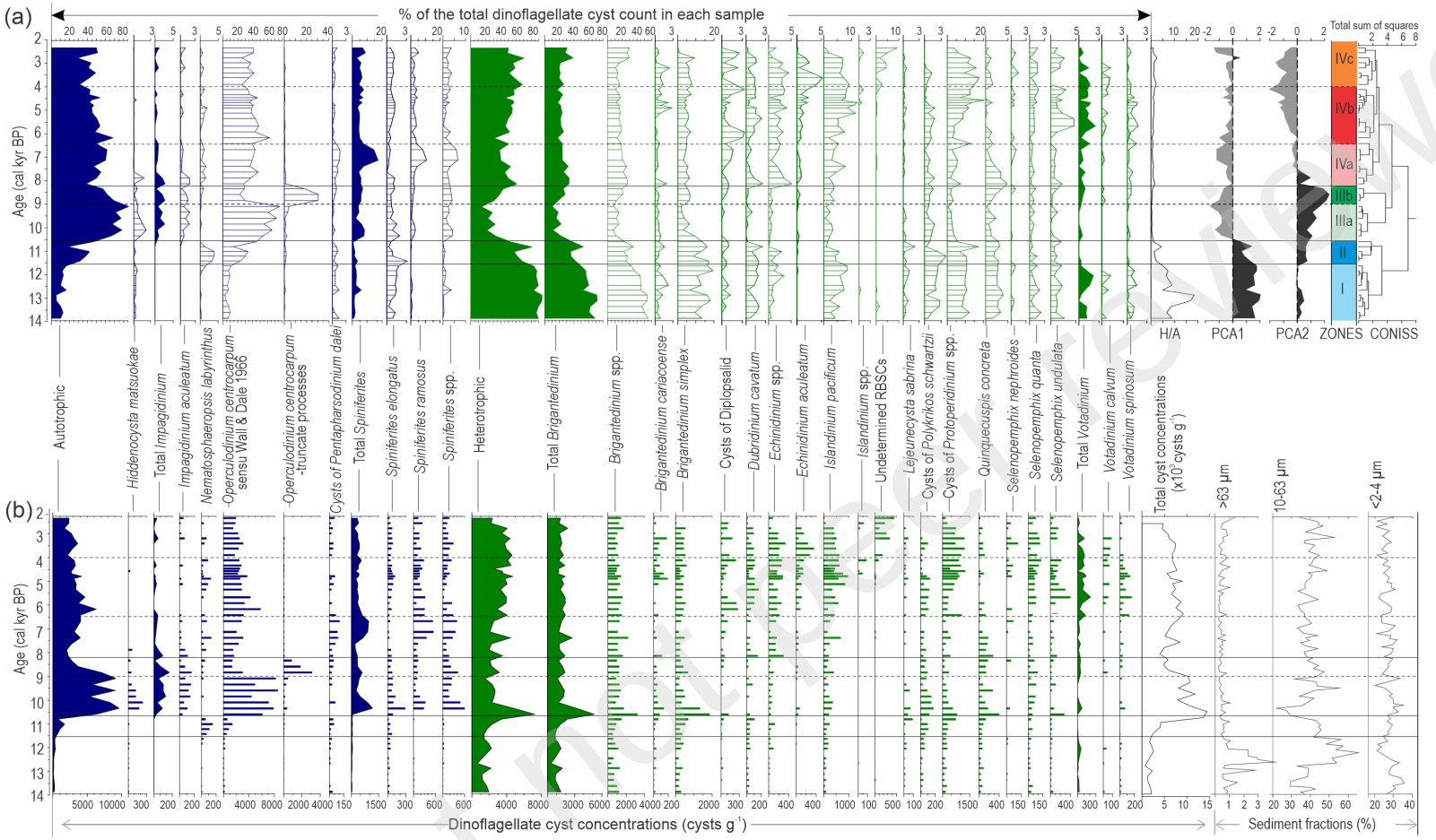

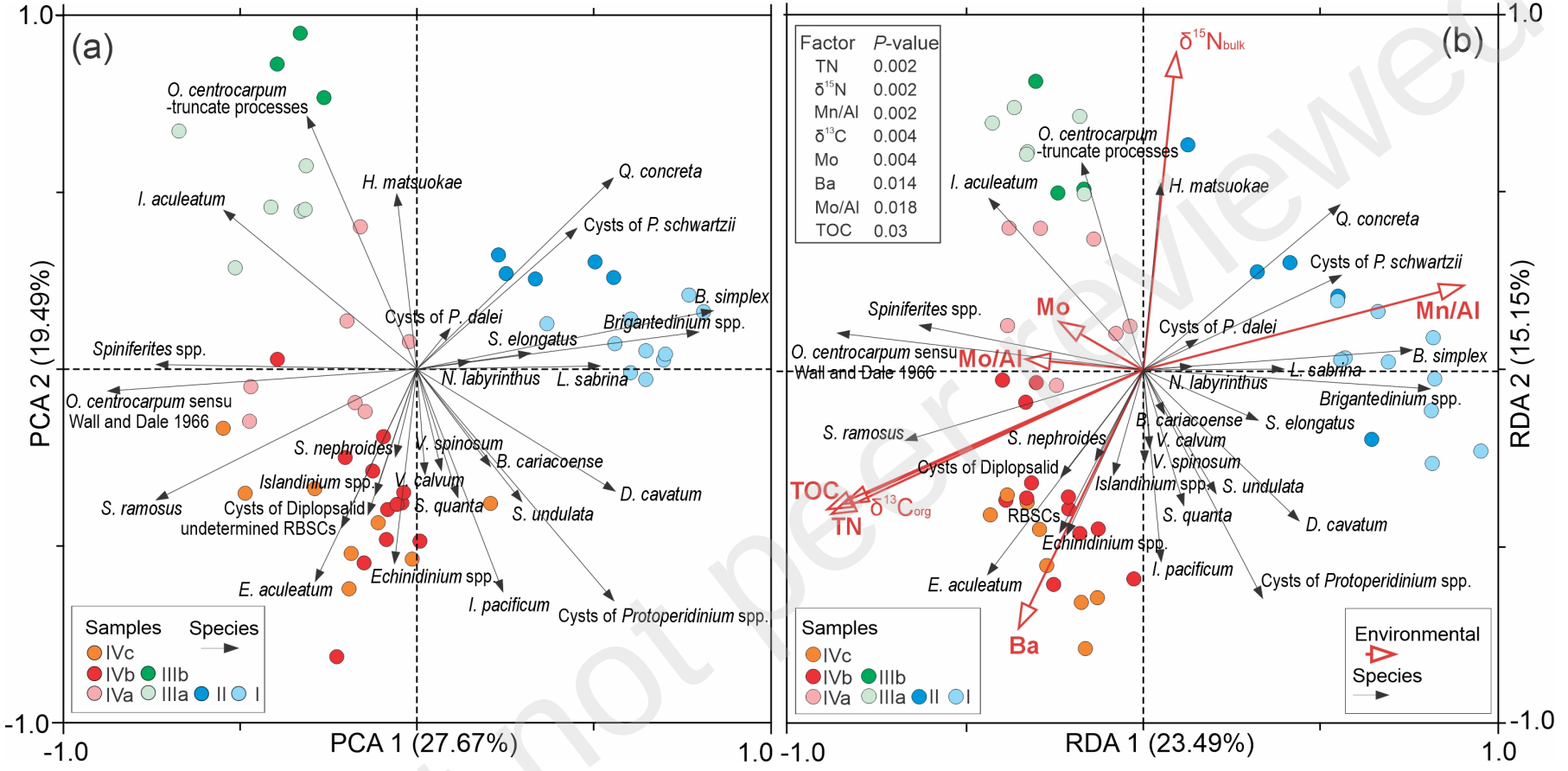

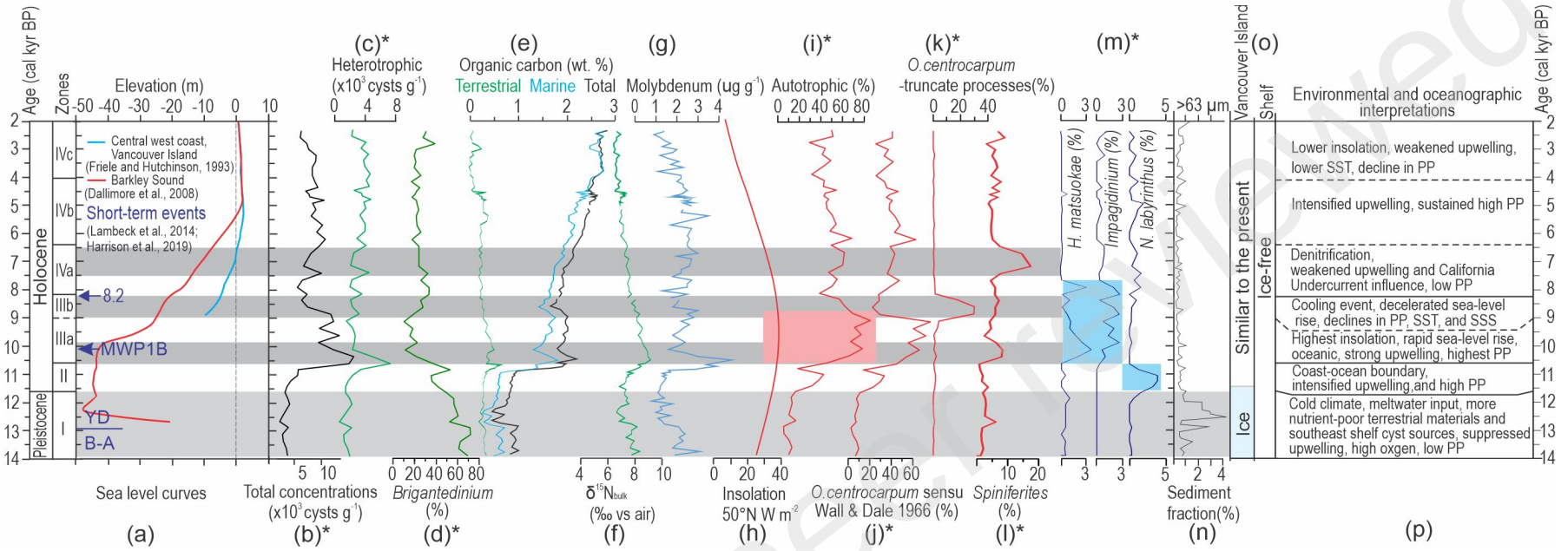

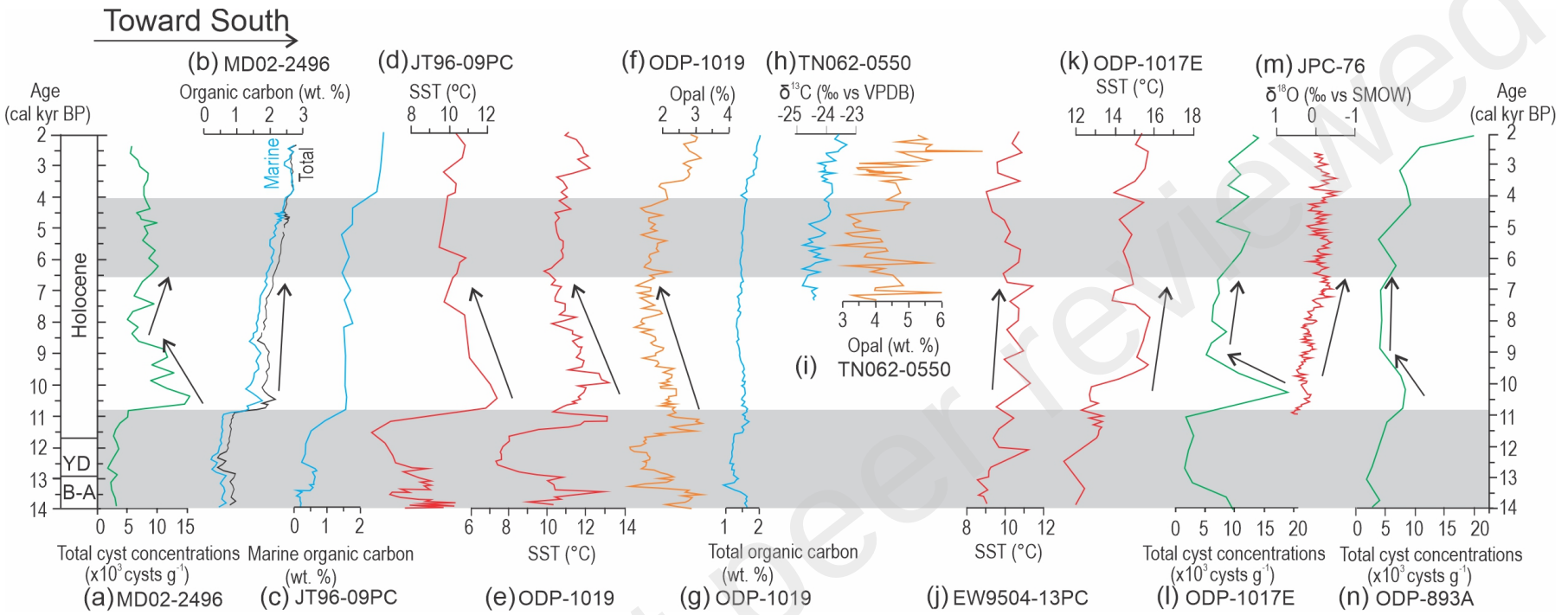

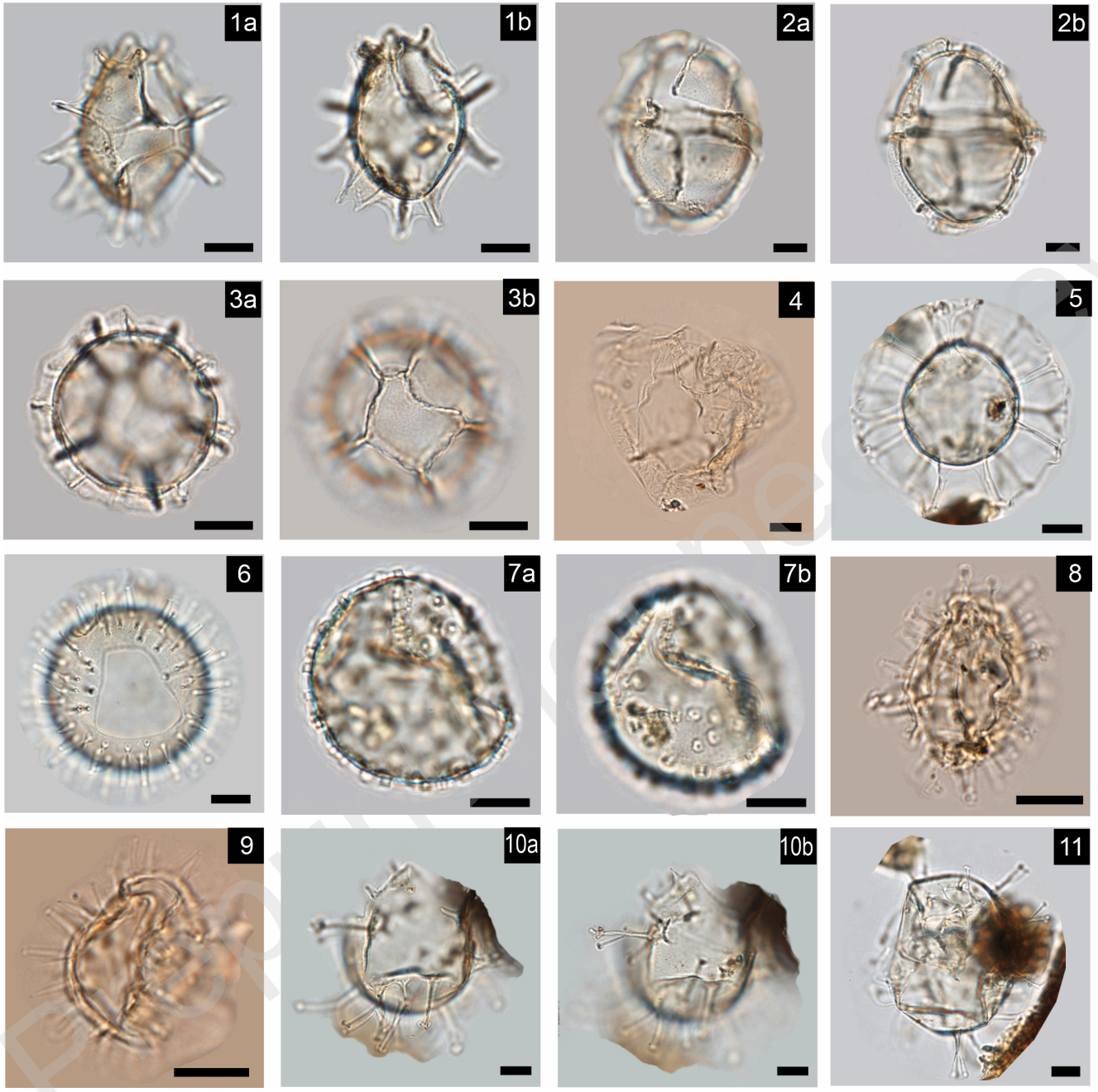

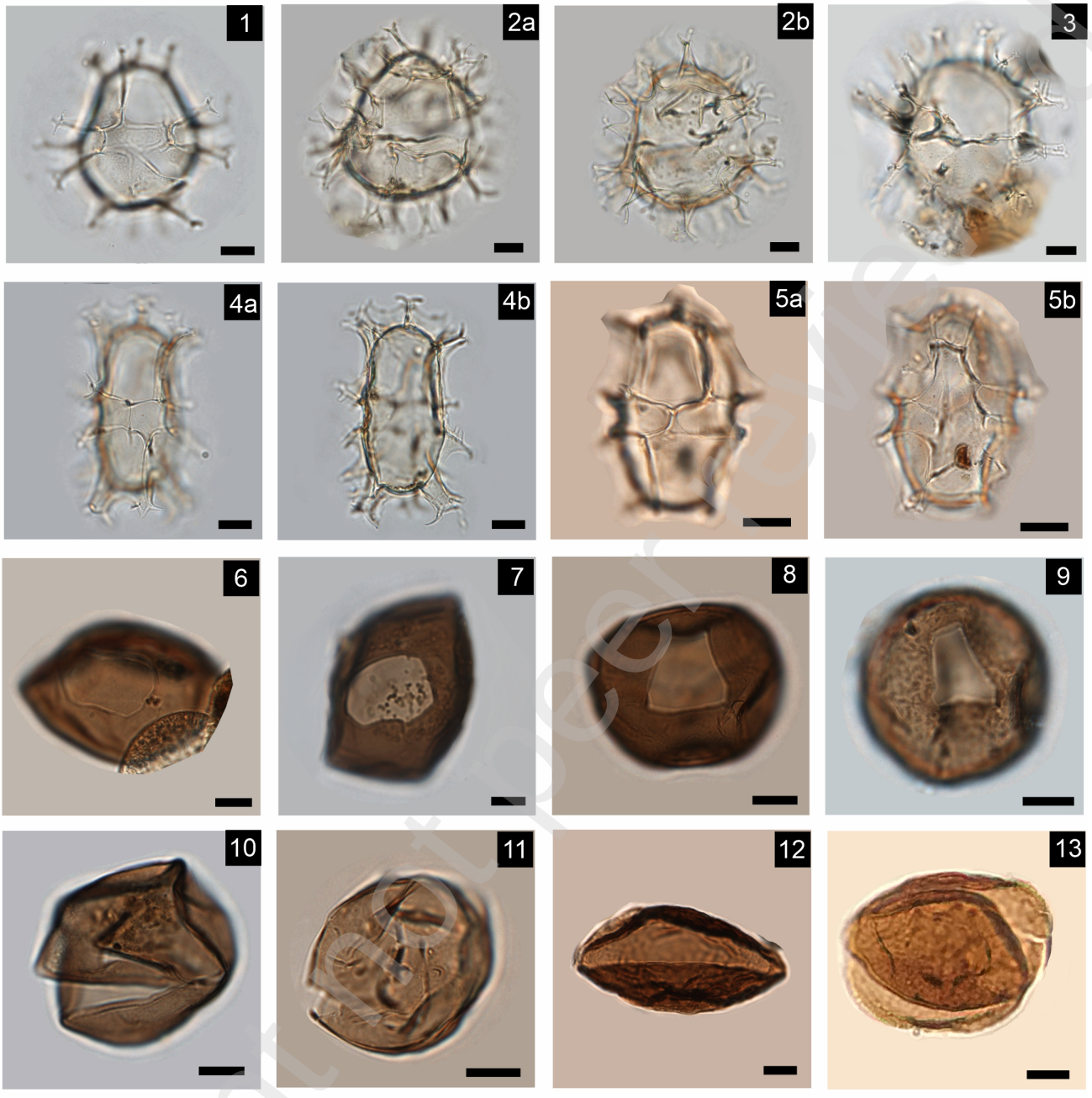

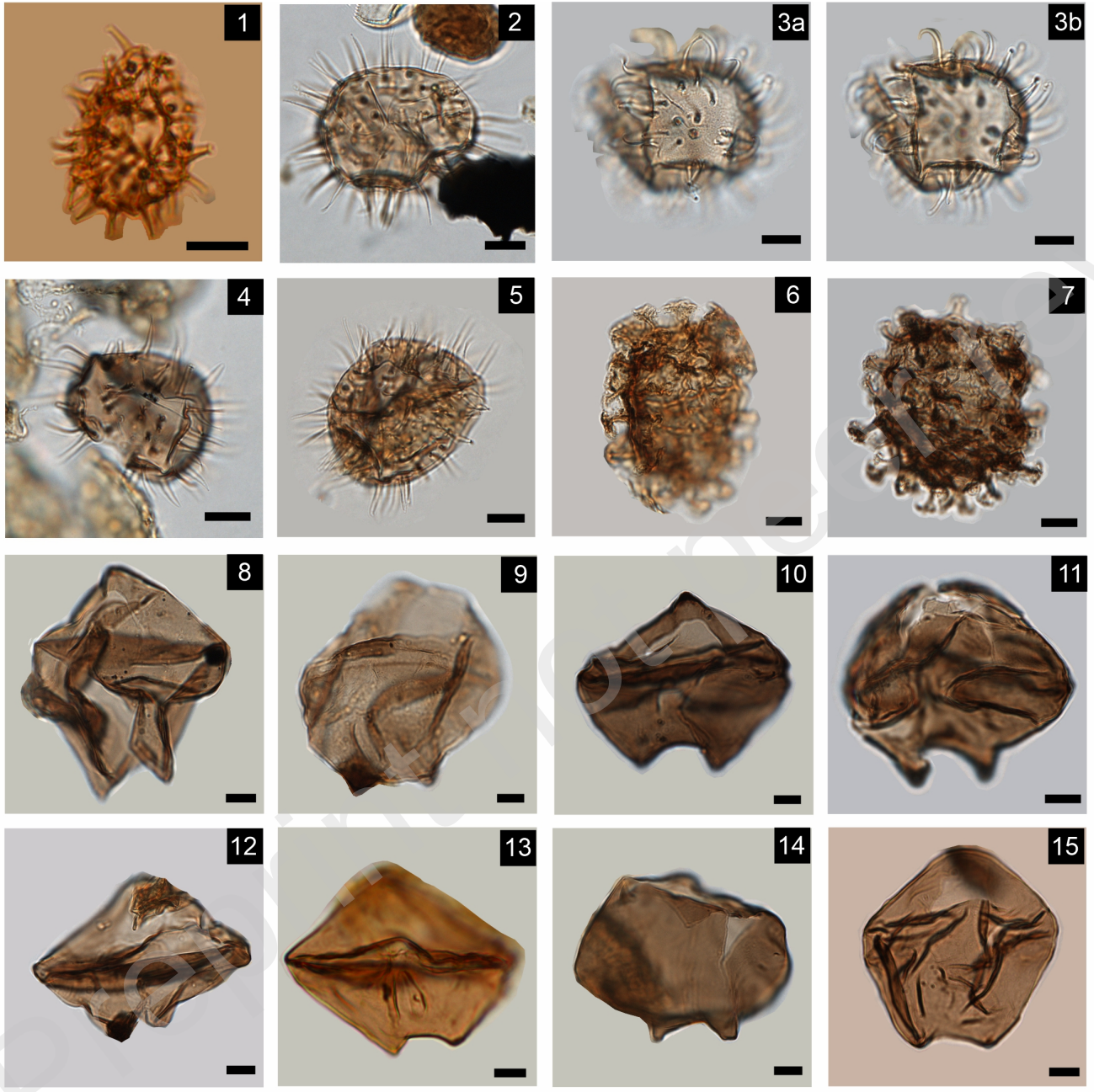

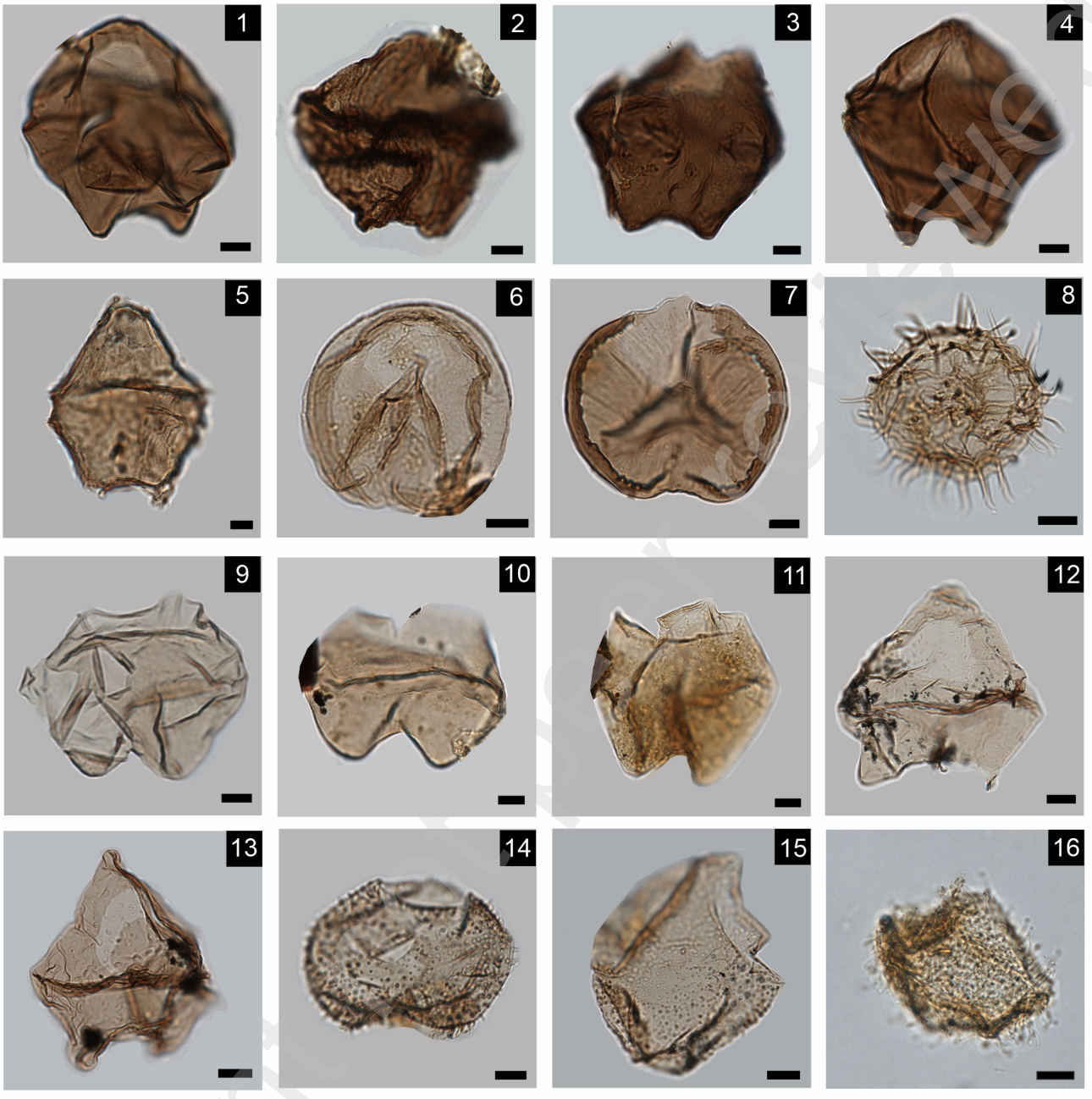

Table 1. List of dinoflagellate cyst taxa identified in this study.

Cyst species (paleontological name)	Dinoflagellate theca or affinity (biological name)
Autotrophic taxa	
Gonyaulacaceae	
Hiddenocysta matsuokae	*Gonyaulax* spp.
Impagidinium aculeatum	Unknown
Impagidinium pallidum	*Gonyaulax* spp.
Impagidinium paradoxum	*Gonyaulax* spp.
Impagidinium strialatum	*Gonyaulax* sp. indet.
Impagidinium spp.	*Gonyaulax* spp.
Nematosphaeropsis labyrinthus	*Gonyaulax spinifera*
Operculodinium centrocarpum sensu Wall and Dale	*Protoceratium reticulatum*
Operculodinium centrocarpum-short processes	*Protoceratium reticulatum*
Operculodinium spp.	Unknown
Spiniferites elongatus	*Gonyaulax ovum*
Spiniferites ramosus	*Gonyaulax spinifera* complex
Spiniferites sp. 1	*Gonyaulax spinifera* complex
Spiniferites spp.	*Gonyaulax spinifera* complex
Perdiniaceae	
Cysts of *Pentapharsodinium dalei*	*Pentapharsodinium dalei*
Heterotrophic taxa	
Diplopsalidaceae	
Dubridinium cavatum	Diplopsalid group
Diplopsalidaceae (or Protoperidiniaceae)	
Cysts of Diplopsalid	Diplopsalid
Echinidinium aculeatum	Diplopsalid or Protoperidinioid group
Echinidinium granulatum	Diplopsalid or Protoperidinioid group
Echinidinium spp.	Diplopsalid or Protoperidinioid group
Islandinium pacificum	*Protoperidinium mutsuense*
Islandinium spp.	*Protoperidinium?*
Undetermined round brown spiny cysts	
Protoperidiniaceae	
Brigantedinium cariacoense	*Protoperidinium avellanum*
Brigantedinium irregulare	*Protoperidinium denticulatum*
Brigantedinium simplex	*Protoperidinium conicoides*
Brigantedinium spp.	*Protoperidinium* spp.
Cysts of *Polykrikos kofoidii*	*Polykrikos kofoidii*
Cysts of *Polykrikos schwartzii*	*Polykrikos schwartzii*
Cysts of *Protoperidinium* spp.	*Protoperidinium* spp.
Lejeunecysta sabrina	*?Protoperidinium leonis*
Lejeunecysta spp.	*? Protoperidinium* spp.
Leipokatium invisitatum	Unknown
Quinquecuspis concreta	*Protoperidinium leonis*
Selenopemphix nephroides	*Protoperidinium subinerme*
Selenopemphix quanta	*Protoperidinium conicum*
Selenopemphix undulata	Unknown
Votadinium calvum	*Protoperidinium latidosale*
Votadinium pontifossatum	*Protoperidinium paraoblongum*
Votadinium spinosum	*Protoperidinium claudicans*
Votadinium spp.	*Protoperidinium* spp.